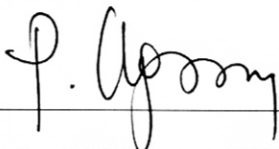


RAPID 3D SCENE RECONSTRUCTION FROM KITE-BASED AERIAL IMAGERY  
USING OPEN SOURCE STRUCTURE FROM MOTION

by

Michael Roy Resig  
A Thesis Project  
Submitted to the  
Graduate Faculty  
of  
George Mason University  
in Partial Fulfillment of  
The Requirements for the Degree  
of  
Master of Science  
Geoinformatics and Geospatial Intelligence

Committee:

 _____	Dr. Arie Croitoru, Thesis Director, Associate Professor
 _____	Dr. Matthew Rice, Committee Member, Associate Professor
 _____	Dr. Sven Fuhrmann, Committee Member, Associate Professor
 _____	Dr. Anthony Stefanidis, Committee Member, Professor
 _____	Dr. Anthony Stefanidis, Department Chair
 _____	Dr. Donna M. Fox, Associate Dean, Office of Student Affairs & Special Programs, College of Science
 _____	Dr. Peggy Agouris, Dean, College of Science
Date: <u>December 5, 2014</u>	Fall Semester 2014 George Mason University Fairfax, VA

RAPID 3D SCENE RECONSTRUCTION FROM KITE-BASED AERIAL IMAGERY  
USING OPEN SOURCE STRUCTURE FROM MOTION

A Thesis Project submitted in partial fulfillment of the requirements for the degree of  
Masters of Science at George Mason University

by

Michael Roy Resig  
Bachelor of Arts  
Wheaton College, IL 2009

Director: Arie Croitoru, Professor  
Department of Geoinformatics and Geospatial Intelligence

Fall Semester 2014  
George Mason University  
Fairfax, VA



**THIS WORK IS LICENSED UNDER A [CREATIVE COMMONS  
ATTRIBUTION-NONCOMMERCIAL 3.0 UNPORTED LICENSE](https://creativecommons.org/licenses/by-nc/3.0/).**

## **DEDICATION**

This is dedicated to my loving and wonderful wife Hannah. Your continual support has motivated me throughout the years to keep chasing my passions and enjoy life. Also to my family, who always taught me to pursue my interests with vigor and integrity and supported me every step of the journey.

## **ACKNOWLEDGEMENTS**

I would like to thank the many friends, coworkers, and supporters who have helped make my degree and thesis possible. Without them, I would not have had the opportunity to pursue this degree. Dr. Matt Rice, Dr. Arie Croitoru, and Dr. Anthony Stefanidis were pivotal in guiding and educating me during my Master program. Finally, I would like to thank my past professors and mentors for guiding me to where I am today. Their dedication to education and excellence gave me the tools to excel at life and learning.

## TABLE OF CONTENTS

	Page
List of Tables .....	vii
List of Figures .....	viii
List of Abbreviations .....	ix
Abstract .....	x
Chapter One: Introduction .....	1
1.1 Motivation .....	1
1.2 Problem Definition .....	2
1.3 Thesis Objectives .....	3
1.4 Thesis Organization .....	4
Chapter Two: Related work .....	6
2.1 Relevant Fields .....	6
2.2 Overall Methodology .....	9
2.3 Aerial Systems and Imagery .....	11
2.4 Structure from Motion .....	12
2.5 3D Reconstruction .....	13
Chapter Three: Method Application .....	16
3.1 Overview .....	16
3.1.1 Location .....	18
3.1.2 Schedule .....	20
3.1.3 Process Workflow .....	23
3.2 Data Capture .....	24
3.2.1 Equipment .....	24
3.2.2 Setup and Planning .....	28
3.2.3 Capture Procedure .....	31
3.2.4 Upload and Conversion .....	33
3.3 Structure from Motion .....	34

3.3.1 Equipment.....	34
3.3.2 Setup and Preparation.....	35
3.3.3 SfM Algorithm .....	38
3.3.4 Point Cloud Export .....	44
3.4 3D Reconstruction.....	45
3.4.1 Equipment.....	46
3.4.2 Setup and Planning.....	47
3.4.3 Algorithm Application.....	51
3.4.4 Texture Application.....	54
Chapter Four: Results .....	56
4.1 Overview .....	56
4.2 Data .....	58
4.3 Structure from Motion.....	61
4.4 3D Reconstruction.....	65
4.5 Accuracy Comparison.....	69
4.6 Concept Applications .....	73
Chapter Five: Conclusion & Future Research .....	78
Appendix A.....	90
Appendix B.....	91
References.....	92

## LIST OF TABLES

Table	Page
Table 1 - Workflow time.....	56
Table 2 - Project Costs.....	58
Table 3 - Data Table .....	61
Table 4 - Output datasets .....	71

## LIST OF FIGURES

Figure	Page
Figure 1 - Study Site: Green Acres Center facility and surrounding area .....	19
Figure 2 - Simple Workflow .....	23
Figure 3 - Complex Workflow.....	24
Figure 4 - Aerial platform: Delta performance kite .....	25
Figure 5 - GoPro Hero 3 Black Edition .....	27
Figure 6 - GoPro wireless directory.....	31
Figure 7 - VisualSfM Toolbar.....	36
Figure 8 - Step A.....	37
Figure 9 – Image thumbnails and Log .....	38
Figure 10 - VisualSfM: SIFT example .....	39
Figure 11 - Step B.....	40
Figure 12 - Step C.....	41
Figure 13 – Step C: VisualSfM Sparse Reconstruction.....	42
Figure 14 - Step D.....	43
Figure 15 - Dense point cloud.....	44
Figure 16 - MeshLab Toolbar .....	47
Figure 17 - MeshLab UI .....	48
Figure 18 - MeshLab: Dense point cloud .....	50
Figure 19 - MeshLab Poisson's parameters .....	51
Figure 20 - Poisson results.....	52
Figure 21 - MeshLab Parameterization.....	53
Figure 22 - MeshLab Project Texture.....	54
Figure 23 - Final Model with Texture.....	55
Figure 24 - Camera view from 70 feet altitude.....	60
Figure 25 - Results: Step A.....	62
Figure 26 - Results: Spanning tree and Match matrix .....	63
Figure 27 - Results: Step C .....	64
Figure 28 - Results: Dense Point Cloud.....	65
Figure 29 - Results: Dense Point Cloud 2.....	66
Figure 30 - Results: Steps H, I.....	67
Figure 31 - Step J: Textures .....	68
Figure 32 - Georeferencing Model .....	70
Figure 33 - 500 ft kite altitude .....	83

## LIST OF ABBREVIATIONS

Three-dimensional .....	3D
User Interface .....	UI
Area of Interest .....	AOI
Geographic Information System .....	GIS
Digital Elevation Model.....	DEM
Global Positioning System.....	GPS
Root Mean Square.....	RMS
Structure from Motion .....	SfM
Scale Invariant Feature Transform.....	SIFT
Clustering Views for Multi-view Stereo.....	CMVS

## **ABSTRACT**

### **RAPID 3D SCENE RECONSTRUCTION FROM KITE-BASED AERIAL IMAGERY USING OPEN SOURCE STRUCTURE FROM MOTION**

Michael Roy Resig, M.S.

George Mason University, 2014

Thesis Project Director: Dr. Arie Croitoru

There has been a significant increase over the past decade in worldwide demand for rapid and efficient capturing of 3D geospatial data. Until recently the technology and training essential to acquire 3D geospatial data was severely limited to government agencies or large corporations. Increasingly affordable tools and methods have given 3D geospatial capabilities to the public, which can be observed within numerous fields of research and industry, such as: military operations, emergency response, humanitarian aid, municipal upkeep, topographic surveying, and cultural heritage. With applicable 3D data the ability to visualize surroundings, perform simulations, conduct crucial research, and gain invaluable knowledge becomes possible. This thesis focuses on developing an accessible, affordable workflow for rapidly creating 3D scenes constructed from captured image series by an aerial platform. By using open source software and simple to operate aerial

vehicles such as kites, this workflow is able to be used in nearly any application while requiring minimal training and funding.

## **CHAPTER ONE: INTRODUCTION**

### **1.1 Motivation**

The adoption and implementation of 3D geospatial data by almost all major industries has significantly increased the demand for the ability to quickly and efficiently capture, create, and visualize 3D environments in an economical manner [1]. With applicable 3D data the ability to visualize surroundings, perform simulations, conduct crucial research, and gain invaluable knowledge becomes possible. A few applications of 3D environment data that are prominent within industries are: military operations, humanitarian response, and municipal upkeep. For military operations knowledge of the battlefield or transportation route is essential for troop safety. Using aerial sensors and imagery, detailed 3D reconstructions are created at nearly real-time rates to provide critical intelligence for squads and commanders. Applications such as viewshed and line-of-site allow informed decisions to be made for deploying and moving troops. During humanitarian response operations, using 3D reconstructions of the region in distress can allow precise zones to be targeted for airdrops or ground relief while taking into account the surrounding terrain, structures, potential hazards, and open clearings for bivouacs. Local governments and municipal organizations constantly monitor and zone their jurisdictions. Using 3D reconstructions of the neighborhood allow educated planning and zoning decisions by considering the surroundings. Local real estate is also able to use 3D

scenarios to model the environment of a single plot or an entire neighborhood, further enlightening buyers, sellers, or municipal regulations.

## **1.2 Problem Definition**

Most individuals and research teams do not have the time, ability, or financial means to acquire high-quality 3D data that pertain to their specific needs, aside from purchasing 3D data from large corporations and companies such as Google [2]. For example, a university's cultural heritage expedition would substantially benefit from a 3D reconstruction of their historical site-of-interest, but they cannot acquire the proper equipment or even training to use the necessary tools. 3D scanning capable equipment that is often used by larger industries which includes laser scanners, drones, and LiDAR systems, can dramatically range in price and operational training, which severely limits access. In response to the limitations of cost and expertise with acquiring commercial 3D geospatial data, simpler techniques of acquisition have developed focusing on using more cost and time efficient methods. One of the most recent advances in cost and time efficient 3D geospatial data utilizes structure-from-motion (SfM) to create data for potential 3D environments. SfM has been used within computer science for over a decade and its potential applications to 3D reconstruction have been widely researched. Due to computationally heavy algorithms, SfM witnessed restricted use on most commercial computers through the 2000's. SfM has only recently been introduced to the public domain in the form of media exploration applications, such as Microsoft's Photosynth

and AutoDesk's 123D. With the resurgence of SfM as an accessible method of 3D reconstruction there are numerous opportunities to explore its geospatial application.

A significant geospatial application for SfM is to utilize live-feed aerial imagery and additional 3D meshing techniques to produce near real-time 3D reconstructions of an environment. Most affordable forms of aerial imaging, such as balloon and kite mapping, do not use streaming or wireless capabilities with photo capture equipment. In addition, the post-processing of the aerial imagery is usually performed in a lab space hours or days after the imagery capturing occurred. By improving the workflow using current technologies and algorithms the process of data acquisition, aerial imagery processing (SfM), and 3D reconstruction could be fully automated and produce near real-time visual results.

### **1.3 Thesis Objectives**

The advancement of cost and time efficient 3D mapping capabilities is a growing field of research within geospatial sciences. The issue of costly hardware and steep operational training curves with 3D mapping devices severely limit the accessibility of 3D data to many industries and applications. The goal of this research is to demonstrate a concept for a time and cost efficient method for capturing high resolution aerial imagery and producing rapid 3D data using aerial vehicles (kite) that are cheap and simple to operate. The ability to produce real-time 3D environments using SfM from aerial imagery at a time and cost efficient level has yet to develop within the geospatial sciences. SfM has been robustly researched within the fields of computer science, mathematics, and

engineering, but using SfM with aerial imagery to reconstruct 3D environments has not received sufficient research publication using recent technological advances. In addition, the process of rapid real-time 3D reconstruction from cost efficient aerial imagery has not been seriously approached as a research topic. This topic is now a viable concept due to recent advances in photo capturing, data transmission, and computing power. Utilizing compact, high-quality, Wi-Fi capable camera equipment with computationally powerful laptops allows for rapid transfer of imagery directly to the platform that processes SfM and 3D reconstruction. This research question will test current SfM methods of 3D data acquisition by applying additional processes, using advanced equipment, incorporating developed algorithms, and integrating supplemental data to produce a rapid real-time 3D environment allowing for speedy validation and utilization.

#### **1.4 Thesis Organization**

The thesis is organized in the following manner. Chapter 2 explores and reviews related work. The related work addressed in this thesis pertains to each individual step within the analyses as well as overall approach to the problem. Chapter 3 elaborates the specific methods utilized within the thesis. Each sub section within the chapter focuses on a specific step in the overall process and the methods applied to accomplish the tasks. Chapter 4 presents and discusses the results generated throughout the method application. The data, variables, and sequential output from each step is presented and validated for accuracy and significance. Chapter 5 provides a conclusive overview of the thesis process

and results. Future applications and research are also addressed relating to the findings presented in chapter 4.

## **CHAPTER TWO: RELATED WORK**

The literature encompassing the thesis research topic spans several disciplines, but relate directly to the geospatial sciences. The procedures to be used in the working demonstration are gathered from the research fields of computer vision, 3D modeling, intelligence systems, emergency response, cultural heritage, and others. A brief review of related literature reveals promising utilization of successful research methods performed by the applicable fields. The first section (2.1) in this chapter establishes a broad foundation detailing the various fields that use elements of aerial imaging, SfM, or 3D model reconstruction. The second section (2.2) reviews related work recently performed and/or published that support the overall methodology and application pursued in this thesis. The remaining three sections (2.3, 2.4, 2.5) review related work recently performed and/or published that specifically pertain to the technical methods applied in this thesis: aerial imagery capture, structure from motion analysis, and 3D reconstruction.

### **2.1 Relevant Fields**

The significant increase in worldwide demand for rapid and efficient capturing of 3D geospatial data has grown drastically in the past decade [1]. Affordable tools and methods have given these capabilities to a much larger population and the effects can be seen within numerous fields of research and industry [3]. With applicable 3D data the ability

to visualize surroundings, perform simulations, conduct crucial research, and gain invaluable knowledge becomes possible. Fields with relevant application concerning this thesis are: military operations, emergency response, humanitarian aid, municipal upkeep, topographic surveying, and cultural heritage [3].

For military operations knowledge of the battlefield or transportation routing is essential for troop safety. Using aerial sensors and imagery, incredibly detailed 3D reconstructions are created at nearly real-time rates to provide critical intelligence for squads and commanders. Applications such as viewshed and line-of-site allow informed decisions to be made for deploying and moving troops. Areas of research advancement within military application have been optimal path computation [4], real time object detection [5], UAV mission planning [6], and rapid 3D environment creation [7].

Emergency response is the most time-critical civilian application of aerial imaging and 3D scene construction. All information produced for emergency response must be produced rapidly and be of utmost accuracy [3]. Applications using drones for overall situational awareness have been deployed for fire response [8]. The necessities of emergency response have driven research concerning the use of low-cost UAV platforms [8], real-time object detection [5], and rapid 3D modeling[7].

During humanitarian response operations, using 3D reconstructions of the region in distress can allow precise zones to be targeted for airdrops or ground relief while taking into account the surrounding terrain, structures, potential hazards, and open clearings for bivouacs [9]. It is unfortunately a common situation that areas in need of humanitarian need do not have sufficient geospatial resources to aid the response [10].

Due to the broad demands of humanitarian response and significant data collection, research has advanced rapid object detection [7], and education and distribution of geospatial results [11].

Local governments and municipal organizations constantly monitor and zone their jurisdictions. The use of aerial imaging and 3D models have become common and reliable tools for municipal improvements. UAVs have been used to monitor traffic, increasing the effectiveness of municipal implementation [12]. Using 3D reconstructions of the neighborhood allow educated planning and zoning decisions by considering the surroundings [13][14]. Effects of impervious materials on the surrounding ecosystem have been researched by utilizing aerial imagery and object detection [15]. Local real estate is also able to use 3D scenarios to model the environment of a single plot or an entire neighborhood, further enlightening buyers, sellers, or municipal regulations [16].

Topographic surveying is a broad application for aerial imagery and 3D modeling and has a far-reaching effect on many people. Advancements in capture technology have vastly improved the accessibility and distribution of topographic survey results. High resolution digital elevation models can be easily created using aerial imagery capture and SfM integration [17]. The overall accuracy of current and past topographic surveys have been assessed using UAV and satellite imagery integration [18]. Large-scale scene reconstruction and surveying is also becoming a viable method of geospatial data accumulation [19].

The fields of cultural heritage and archaeology have greatly benefitted from the increased accessibility of aerial imagery and 3D reconstruction technologies [20]. The

ability to digitally capture environments and objects for permanent record or analysis has expanded the research possibilities within cultural heritage to beyond field work. A significant advancement developed by archaeologists has appeared with the 3D reconstruction of historical and excavation sites using UAV and SfM technologies [2] [21]. Using related techniques, researchers are able to perform non-invasive surveys of entire regions or specific sites [22]. Having a digital record of historical sites ensures that the visual and cultural details of the environment will always be available for future research [11]. Also, the concept of “virtual museums” has now become a viable reality with the capability to digitally reconstruct entire landscapes and objects viewable to the public [23]. Perhaps the most significant development to emerge from this technological revolution is the expansion of archaeology outside of the exclusively academic realm [24].

## **2.2 Overall Methodology**

There are two prominent applications for the related literature: developing research process and workflow, and integrating technical methodology. The overall workflow presented in this thesis is originally developed, but greatly enhanced and inspired by related research. This section looks at the related work performed and published that support the overall methodology and application. The articles by Ducke [2], Lewis [8], Tonkin [17], and current research project by Dr. Block-Berlitz [21] in Germany called “Archaeocopter”, present excellent examples of end-to-end research projects that focus on demonstrating a time and cost efficient aerial imaging system for 3D visualization.

These research projects closely resemble the workflow that is outlined in this thesis. Duce focuses heavily on the full workflow of 3D reconstruction from beginning to end. The article emphasizes the importance of recognizing legislative and financial constraints that many research pursuits endure. The article also highlights the necessity for new technologies to be simple, robust, cheap, and efficient in order to have a positive effect on industries. This approach is directly in line with the goals of this thesis. Multiple freeware and open source components are utilized throughout the tool chain to accomplish the 3D reconstruction, such as Bundler and MeshLab [25][26]. The Lewis research project evaluates the use of low-cost UAVs to capture aerial imagery in emergency response situations. The proposed platform is able to provide timely acquisition of high resolution imagery with very limited flight training for a relatively low cost (\$8,000). This project provides an excellent example of a small-scale research process which utilizes similar beginning-to-end steps to the proposed thesis. Tonkin et al. explore the potential applications of unmanned aerial systems integrated with SfM to develop topographic surveys. This research project successfully communicates the accuracy, precision, and potential applications to their specific surveying approach. This project strives to produce digital elevation datasets that are comparable to LiDAR in accuracy, but with a fraction of the time and monetary cost [27] [28]. The work being pursued by Dr. Block-Berlitz is attempting to demonstrate a near real-time application using an aerial imagery-SfM-3D reconstruction workflow, but most research is still in progress. Majority of research developed by Block's team is published on their website and has been presented at numerous conferences[29], which have been positively received. The common thread

between these overarching projects is the need for interdisciplinary integration of technologies within a geospatial application. These articles serve as guidelines for the structure of the thesis as well as present successful examples to compare and contrast the thesis research.

### **2.3 Aerial Systems and Imagery**

The use of aerial systems within the fields of photogrammetry and remote sensing has drastically evolved in the past decade, using cutting-edge technologies to advance its capabilities. Unmanned aerial vehicles such as drones have transitioned from being highly exclusive property of the defense industry to readily affordable and operational to the public [6]. Within the past five years technologies and methods have developed that push the known boundaries of photogrammetry and remote sensing acquisition and processing methods [3]. This surge of accessible, affordable, aerial vehicle technology and processing equipment combined with publically available and refined computer vision software contribute to the exponential growth of research and applications for aerial systems and imagery [3].

The most common and traditional methods of low altitude aerial imaging are captured using unmanned vehicles which include kite, balloon, blimp, fixed-wing, and rotor aircraft [30] [3]. As mentioned above, the introduction of multi-rotor platforms such as drones into the public realm within the past few years has caused an aerial imaging revolution [31]. The ideal application of UAVs involves the technical precision and autonomous navigation capability that allow efficient capture and flight time. Despite the

advanced technology used with UAV platforms, there are viable options for customers that require minimal training and piloting knowledge to utilize [8][32].

## **2.4 Structure from Motion**

Structure from motion is the automatic estimation of 3D scene structure and camera position calculated from a sequence of images. SfM utilizes computer vision technology to perform algorithms that identify similarities and differences between images and subsequently deduce spatial depth. SfM is an ongoing and active field of research within computer science, requiring algorithm and computationally intense processes. The premise of SfM relies on quality digital photos captured from one or various sources. Studies have been performed using different camera specifications, such as wide-lens, fisheye, stereo, catadioptric, pinhole, and multi-camera systems [33]. With each camera system having its strengths and weaknesses, the quality of most SfM results are relative to the desired outcome.

Due to computationally heavy algorithms, SfM witnessed restricted use on most commercial and public computers through the 2000's [19]. SfM has only recently been introduced to the public domain in the form of media exploration applications, such as Microsoft's Photosynth and Autodesk's 123D [34][35]. With the resurgence of SfM as an accessible method of 3D reconstruction there are numerous opportunities to explore its geospatial application. Two open-source SfM systems that have been developed through university and independent research are Bundler and VisualSfM. These SfM platforms have continually been improved throughout the duration of their existence by ambitious

contributors, making them comparable and sometimes superior to the commercial SfM solutions. A significant contribution to the realm of SfM known as Clustering Views for Multi-view Stereo (CMVS) was developed in 2010 by Yasutaka Furukawa and Jean Ponce [36]. The software they developed is able to take a SfM result as input and significantly increase the visual accuracy and density of the scene for 3D reconstruction. This revolutionary approach to high-density SfM advanced the entire field of computer vision research and 3D reconstruction from imagery. VisualSfM and Bundler both utilize CMVS as optional additional steps within the software. Certain elements of the CMVS pipeline are used for real production purposes by Industrial Light & Magic, Weta Digital, and Google Inc [37]. The SfM algorithms used by VisualSfM are a culmination of years of computer vision research developed by Yasutaka Furukawa and Jean Ponce and other research contributors, compiled into the software environment by Changchang Wu [36], [38]–[40]. VisualSfM also uses a widely approved method of image matching known as Scale Invariant Feature Transform (SIFT). This mathematical approach developed by David Lowe is able to transform image data into scale-invariant coordinates relative to local features, in other words: identify similar pixel groupings and shapes between images [41]. SIFT application has substantially improved the field of computer vision and object detection algorithms, allowing processes such as SfM to flourish.

## **2.5 3D Reconstruction**

Digital 3D reconstruction and model building are vast fields of research and application.

The utilization of some form of 3D digital models can be found in almost every industry

worldwide, such as municipal mapping, national defense, industrial monitoring, and entertainment, just to name a few. There are countless programs that are used commercially and publically for 3D model manipulation, but few are open source and good quality. Two open source software platforms that are used for 3D reconstruction are MeshLab and Blender [26]. MeshLab is a widely accepted open source platform for manipulating 3D environments, models, and point clouds [2], [27], [42]. It contains a simple user interface with limited navigation, but excels with the application of 3D data manipulation and mesh construction. The platform contains a large community of developers and contributors who continually improve and add plug-ins. MeshLab is commonly used for preliminary 3D data optimization and cleaning, but also contains the ability to produce and finalize 3D models with high-resolution photo-realistic textures. Most of the built-in functions available in MeshLab for 3D reconstruction are considered the ideal approach, such as Poisson's Surface reconstruction [43]. The Poisson Equation was originally developed from Issac Newton's law of gravity [44], and was first actively applied towards 3D mesh reconstruction by Kazhdan et al. [45], and since has become an optimal approach to 3D surface reconstruction. Other surface reconstruction algorithms include Marching Cubes, Ball Pivoting, Power Crust, Tight Cocone, and Delaunay Triangle [46]–[49]. All of these algorithms have been designed to reconstruct scenes that can be viewed from every angle, having difficulty with partial objects. Poisson's reconstruction is found to be a universal and rapid reconstruction algorithm able to produce acceptable results with minimal cleaning. The purpose of applying the equation

is to solve an unknown target mesh with known topology (e.g. point cloud) but unknown geometry, resulting in accurate estimations of object surface.

## **CHAPTER THREE: METHOD APPLICATION**

This chapter elaborates the equipment, method, and process for each step of the thesis workflow (see Appendix A). Each section of this chapter systematically details every action performed during the project survey. The results of this workflow are summarized in chapter 4. The chapter is organized as follows: section 3.1 presents an overview of the project location, schedule and overall workflow; section 3.2 details the data capture portion of the project; section 3.3 specifies the procedures used in VisualSfM for the SfM step of the project; and section 3.4 concludes with instructions for creating the final 3D reconstruction of the survey area.

### **3.1 Overview**

The accessibility of consumer-line 3D technologies such as AutoDesk's 123D Catch ("Catch") and Microsoft's Photosynth are advantageous to nearly all applications of 3D scene reconstruction. These programs have the capability to fabricate 3D models of objects or scenes from a series of photographs by using photogrammetry or SfM. The benefits of these software are their ability to perform all steps within the reconstruction pipeline, from photograph capture, to calculations, to rendering. The final results from these commercial solutions have a high likelihood of being satisfactory for visual analysis or rough 3D model construction. The entire workflow of processes in Catch and

Photosynth are considered “black box” or proprietary. Although the simplicity of this software is a significant benefit, the inability for the user to customize or manipulate any step in the process is a significant hindrance. For many applications of 3D modeling such as research, emergency response, and topographic surveying, the specifications for a desired output must be customizable. Until consumer-line 3D technologies allow additional customization and user-input variables, open source alternatives provide the flexibility and personalization needed for precise science.

Despite being streamlined and optimized, consumer 3D technologies such as Catch and Photosynth suffer limitations. First, there are restrictions on the number of pictures that can be used for the 3D reconstruction. When using the mobile application of Catch, the user is limited to a maximum of 40 photos, and the desktop application 70. VisualSfM is only limited in number of photos to the processing power of the computer workstation. Second, the technology and algorithms used within Catch and Photosynth are contained within proprietary online repositories which require the captured photos be uploaded to private servers. During the upload process the original photos are reduced in spatial resolution and digital complexity, which severely limits the overall accuracy and quality of SfM results and final texture projection on rendered models. VisualSfM provides a real-time process log that identifies all algorithms and functions performed. Third, the output 3D mesh and texture map from the commercial programs are given an arbitrary size due to lack of built-in functions to specify a desired output model size. VisualSfM allows metadata variables to be applied when exporting final point clouds and 3D meshes to improve proper scale. Fourth, and most limiting of all is the complete black

box nature of the commercial products. It is essential to understand and follow the process of SfM and 3D model reconstruction in order to full utilize the output results. Without mathematical justification and explicit procedures the results from Catch and Photosynth are merely visual assets without direct scientific applications. Using VisualSfM to perform the SfM process on the database of captured imagery optimizes algorithm customization.

### **3.1.1 Location**

The location of interest that is the focus of most aerial imagery data acquisition is the Green Acres Center and property located at 4401 Sideburn Road, Fairfax, VA 22030. This facility presents many opportunities for using aerial photography, most crucial being an open area with limited vertical obstructions. Although the results of this research should be applicable to all uses of aerial imaging, the conditions for this study were performed in a near-optimal, accessible, safe environment. There are numerous locales within the AOI to test the research process upon, such as: residential suburban, large commercial facilities, institutional facilities, large storage buildings, transportation features, industrial/infrastructure features, and sparse forest/fields. The overall accuracy of the research method will be vetted against surveyed CAD datasets of most of the surrounding structures within the GMU campus and housing complexes (Table 3).



**Figure 1 - Study Site: Green Acres Center facility and surrounding area**

There are three steps that should be consulted when determining a good site to perform kite aerial imaging [50]. 1. Identify an open launch site. 2. Observe patterns in wind direction. 3. Determine launch site in relation to mapping target. Steps 1 and 3 were determined through surveying and presented an ideal pairing of nearby launch site and target mapping area. Step 2 is clearly the more variable factor, but predominant wind direction comes from the south and blows in a north-northwest direction ranging from 5-10mph at the ground surface. A minimum wind speed of 5mph is required for a

successful kite liftoff with the additional 2.6oz of camera equipment. Further observation of the target AOI revealed advantageous wind funnels and choke points that were created from the community building and tree lines.

A mandatory step that must be taken when aerial imagery is involved is referencing FAA regulations. Being situated so close to Washington D.C., which prohibits UAV flight and aerial imagery, it is especially important to adhere to uncommon federal regulations. Research has determined that the flying of kites according to the common standards being used in this study are well within the acceptable federal aviation regulations, such as: <500ft kite altitude, daytime operation, operator presence, and acquisition of proper permissions for kite operation [51].

### **3.1.2 Schedule**

The project execution was divided into three main phases (see Appendix B). Phase 1 concerned the development of an adequate aerial imaging platform and the acquisition of an imagery dataset for later analysis. Phase 2 focused on the utilization of SfM techniques for preparation of data and subsequent 3D reconstruction techniques for visualization. Phase 3 focused on refining a workflow between all steps and concluding integration of phases 1 and 2.

Phase 1 of the research project began by testing ideal methods of aerial photography methods within the field. The decision to use a kite for the project is for several reasons: cost effective, minimal training required to pilot, relatively navigable, and accepted culturally worldwide. These simple reasons promote the use of a kite for

easy and cost-efficient aerial photography. Alternate photo capture techniques were considered as potential supplements to producing adequate datasets. The kite was attached with a sufficient camera and a wireless uplink connected to the processing workstation. The camera produced multiple copies of the digital data collected, one copy on the micro SD card within the camera, and the second copy wirelessly transferred in real-time to the workstation. The designated study site, Green Acres Center (Figure 1), presented an ideal location for aerial platforms and data validation with agreeable weather conditions and public availability.

Multiple field work sessions occurred throughout the project duration. Initially a large imagery dataset was successfully acquired using the proposed methods. This initial data in digital format was used as the primary image dataset for later SfM and 3D reconstruction steps. Phase 3 required additional active field work collection of aerial imagery to demonstrate a working example of the proposed end-to-end rapid real-time 3D reconstruction workflow. The thesis schedule offered flexibility to allow additional field work to occur if necessary.

Phase 2 encompassed the analysis of imagery using SfM and 3D reconstruction techniques. The goal of this phase was to demonstrate a workflow with minimal user input that performs SfM and produces an acceptable 3D reconstruction from the captured imagery dataset. This phase will utilize open source and freeware platforms to execute the analysis. Most of the SfM platforms mentioned (see section 2.4) have been developed by rigorous research labs and are capable of executing the necessary algorithms with optimal speed and simplicity. The SfM process ingests all relevant aerial images from the

dataset and using the accepted algorithms, produce a point cloud representing a sparse model of the captured environment. The point cloud data is then imported into the 3D rendering and reconstruction platform for final visualization (



). The final 3D rendering ideally has potential use for future applications. A personal laptop was utilized as an ideal field work device, containing medium-high processing power and RAM ratings and wireless compatibility. During phase 2, most of the processing and analysis occurred on PC to ensure data and method integrity. The resulting workflow and procedure demonstrated from this phase was developed for compatibility with the laptop environment to perform the phase 3 integration.

Phase 3 integrated the processes demonstrated in phase 1 and 2 into a continuous workflow capable of visualizing 3D environments. The result of this final phase demonstrated an end-to-end method capable of capturing aerial imagery via kite, transferring the imagery rapidly to a workstation, processing the imagery with SfM, and rendering a 3D environment, all done in rapid succession. The challenge of this phase was to ensure that each step of the workflow was running correctly and producing the desired results. Ideally, the final workflow will be able to automatically proceed through each step of the process with minimal user interaction, made possible through future research.

### 3.1.3 Process Workflow

The process workflow presented in this thesis was developed specifically to perform the intended tasks using the data, software, and hardware outlined prior. A general synopsis of the process workflow is given in this section (**Error! Reference source not found.**), with extensive details provided in the remaining sections of the chapter and workflow shown in Figure 3. The simple process workflow is: data acquisition, SfM analysis of the image dataset, and 3D model reconstruction. All data acquired for the research will undergo post-processing or conversion, quality inspection, SfM analysis, removal of redundancies or incompatibilities, and point cloud construction. The completed SfM results and point clouds are then combined to form a cohesive 3D environment or model. Further research will determine the capability of implementing more rapid processing of the imagery into 3D environments.



Figure 2 - Simple Workflow

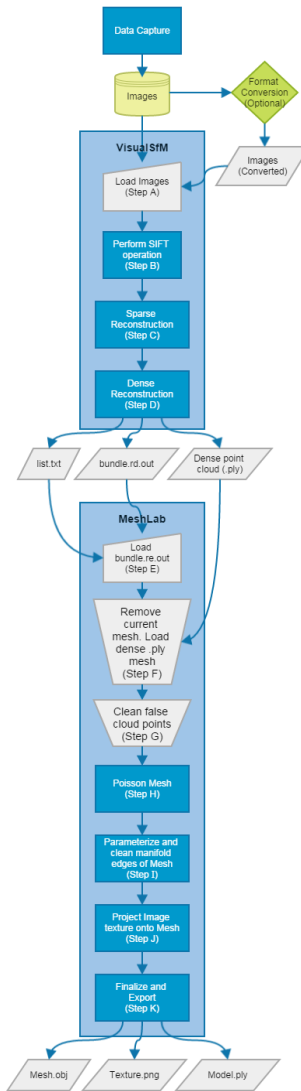


Figure 3 - Complex Workflow

## 3.2 Data Capture

### 3.2.1 Equipment

The equipment used for the data capture portion of the thesis encompasses three items: aerial vehicle, imaging apparatus, and connecting harness. The main aerial vehicle used in this research project is the kite (Figure 4). The primary kite used in this project is a

high-performance delta sport kite with two controlling lines. The delta shape is a common kite design used within kite mapping communities due to its lift and maneuverability [50]. The decision of using a performance kite was initiated by the researcher, having previous experience with such aerial vehicles and realizing their benefits. The maneuverability of the performance kite allows advanced motion, perspective, and active imagery capture. This added capability of precise steering reduces the time and effort needed by using traditional kites, which rely more on weather and wind behavior. In addition, alternate delta-kite and anchored balloon vehicles were briefly used in the field research for comparison. Sufficient string for anchoring the aerial platform is also desired. Spools in excess of 300 feet with a tensile strength greater than 75 pounds are used.



**Figure 4 - Aerial platform: Delta performance kite**

When determining the proper aerial vehicle to use for a field survey, specification of the area of interest (AOI) must be identified. There are certain questions that can help

determine adequate vehicle applicability, such as: how large of an area is being surveyed? Are there limitations or obstructions to aerial vehicles? Is there an open area sufficient for aerial vehicle mobility? Are there legal or personal restrictions for surveying the site? Are weather conditions favorable for aerial vehicle usage? These questions can help narrow the possible aerial vehicle options available.

This research project uses the GoPro Hero 3 Black edition (Figure 5). There are numerous viable options for digital camera equipment [50]. Although there is no consensus determining an ideal camera platform, there are a few preferred cameras that are highly recommended by researchers and enthusiasts [52]. The model of camera depends on the capture quality desired and aerial vehicle lift capacity. In most cases there is a tradeoff between size and weight of a camera and the quality of images captured. The optimal camera selection should allow the best quality image performance while still navigable on the aerial vehicle. The GoPro is ideal for aerial platforms due to its incredibly lightweight frame (73 grams) and durability. It also has capture capabilities on par with larger cameras, such as time-lapse, wide angle lens, video, and high resolution up to 12 megapixels. It has wireless control and uplink abilities, making it an ideal camera for this research project.



**Figure 5 - GoPro Hero 3 Black Edition**

The apparatus for connecting the camera to the aerial vehicle combines GoPro protective casing and adjustable material (Figure 5). Being a highly mobile aerial platform the connecting apparatus must be durable, stable, and flexible [50]. There are various solutions to mounting a camera on aerial platforms offered by researchers and enthusiasts. For kite photography, a common apparatus involves an empty plastic bottle - a solution that is simple, affordable, and reliable [50]. As stated above, the most significant limitation to aerial platforms is the weight restriction imposed by adding a camera. The increase in weight reduces the stability and control of the aerial vehicle while increasing the demand for lift. The solution for this project incorporates a lightweight, bare-minimum harness developed for this situation. The harness uses the backing from the GoPro plastic protective casing and is fastened to the central support frame of the kite using articulated wire. The camera is held in the plastic backing with at least three rubber constraints to ensure a firm hold while allowing easy removal. The weight of the camera is fully supported by the wire, and additional stability is provided

by strings anchoring the harness to more portions of the kite frame. The harness allows adjustments for both oblique and nadir image capture. Attachment and removal of the apparatus requires minimal time or adjustment.

The workstation used in this research project is an HP Pavilion laptop dv6, which contains an i7 quad-core processor, 4 gb DDR3 ram, nvidia graphics card with Cuda, 250 gb hard drive, wireless card adapter, and uses Windows 7 operating system. The components highlighted above are crucial for the computer and are highly recommended for most of the steps in this study (image transfer, SfM algorithm, 3D reconstruction) [53]. All of these computer aspects are essential to perform this study, but varying levels of capability are allowable. Having a high-performing, multi-core processor and more ram will display the most significant improvement in workstation functions. Some of the open source programs and scripts used later in the study may not function properly on a Mac or Linux system. Using a laptop is essential for portability and processing in the field. The wireless card allows the workstation to communicate with the camera (GoPro) which has an internal Bluetooth-compatible wireless network, allowing wireless transfer of images. It is recommended to have charging capabilities on-hand during field work sessions in case of substantial battery loss.

### **3.2.2 Setup and Planning**

The ideal setup for the capture procedure requires all aforementioned equipment, sufficient power, wireless connectivity, and access to the survey AOI. Having determined the survey location and gained surveying permission, optimal weather and lighting

conditions must be projected [50], [52]. With a couple potential dates selected having optimistic weather conditions the schedule is arranged. All equipment must then be prepared.

The GoPro camera has a wide variety of capture settings which greatly ease the process of image acquisition. The significant setting which is used in this project is ‘time-lapse’, allowing the camera to automatically take a picture every ‘x’ seconds, from ‘0.5’ to ‘1 min’. Once activated, this setting will continuously capture and feed images to the workstation wirelessly. In an ideal situation, a high-definition video feed would be optimal, but the degree of technology and wireless bandwidth required is superior to the goals of this research project. A balance between the quantity and quality of images must be determined due to limitations on the speed of wireless transfer between devices. The optimal balance of image capture frequency is deemed acceptable from 1 to 3 seconds between pictures.

The primary dataset required for performing SfM and 3D reconstruction must be composed of a series of compatible images, in this case the GoPro images are JPEG. The quality of image must be established prior to collection, and should be determined by the pixel resolution of the image. The higher spatial and pixel resolution of images will result in higher fidelity surface reconstruction and final texture application [53], [54]. Two resolution settings are used in this study, 12 megapixel wide-lens, and 5 megapixel medium-lens. Depending on the camera system, the lens used may cause visual alterations to the image, such as pin-hole or fisheye effect. These visual effects are easily removed after capture through batch filters to ensure accurate visual representation of the

scene. Graphic editing software such as GIMP, which is freeware found online at <http://www.gimp.org>, is capable to solving these lens distortions. Some SfM platforms are capable of processing raw images that contain skewed lens alterations.

The camera system and workstation must have the proper setup to allow wireless transfer of images. The GoPro system must have been properly set up upon initial activation. If so, the GoPro has wireless capability simply by activating the wireless setting, which is done manually or via remote control. Similarly, the workstation must have the basic wireless functionality established prior to device connection. The GoPro creates its own wireless network which appears as a network option on the workstation. Once selected, the GoPro network requests the previously established password for successful connection. There are numerous ways to transfer images from the GoPro, the fastest being through direct link with a USB cable. If all other methods fail, using the USB cable on-site is a viable option with rapid results. The wireless transfer of imagery is an optimal situation for continuous surveying and scene reconstruction, and is a goal of this research project. Using a windows explorer window, the GoPro device storage can be accessed via the ip address: //10.5.5.9:8080 (Figure 6). Direct access to the camera storage allows immediate transfer of the captured images to the workstation hard drive by using simple copy scripts.

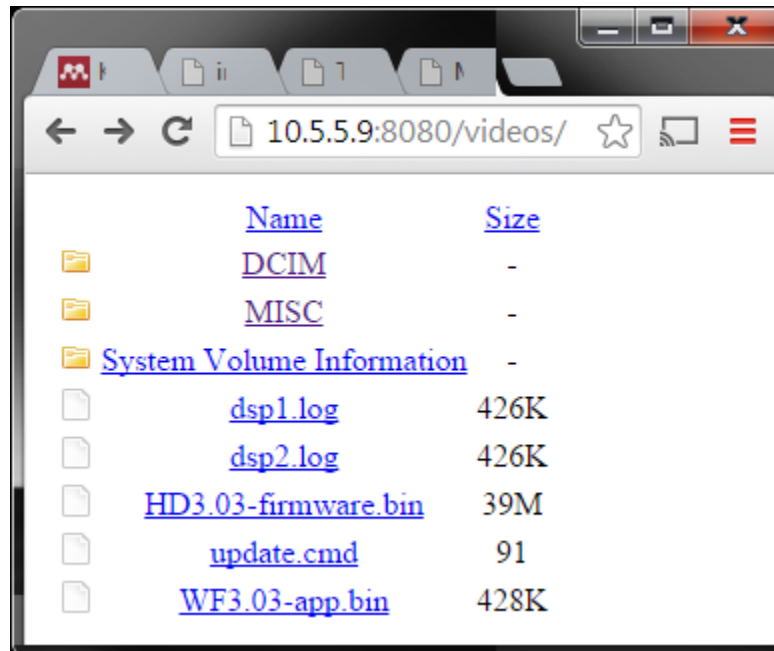


Figure 6 - GoPro wireless directory

The workstation should have maximum processing functionality activated, and if possible, plugged in. The transfer of images over wireless and later SfM and 3D reconstruction demand full workstation attention. The workstation needs to have sufficient hard drive space to store the raw images transferred from the GoPro and later SfM and 3D models. A dedicated folder is created on the hard drive to store the raw images transferred from the GoPro. This separate folder ensures the image series integrity with later processes that might alter the source image.

### 3.2.3 Capture Procedure

Upon completing setup on site, aerial surveying commences. Multiple field work sessions occurred within the duration of this project, with aerial surveying successfully

accomplished with single and dual teams. Regardless of survey team size, the capture procedure remains nearly identical, and is as follows:

- a. Verify device power and wireless connections: GoPro, Workstation.
- b. Position the aerial vehicle (kite) downwind of the navigator.
- c. (optional) If using manual camera activation, begin time-lapse capturing.
- d. If using remote or smartphone app, begin time-lapse capturing.
- e. Launch aerial vehicle, navigating around AOI.
- f. Monitor the transfer of images on the workstation, adjust flight as needed.
- g. Once desired number of images are captured, land aerial vehicle.
- h. Review transferred images for error and AOI scene gaps.
- i. If more images are needed, repeat steps until results are satisfactory.

Each of the numerous surveys performed for this project successfully captured over 100 usable images and were completed in less than an hour. For other project surveys depending on location, weather conditions, and flight success, other field sessions may need to be scheduled.

There are additional capture techniques to consider when acquiring images for SfM. The image series needed for optimal SfM processing requires a different approach than traditional photography. The following is a list of guidelines for proper image acquisition compiled from sources [49], [54], [51]:

- a. SfM projects need a minimum of 3 images to run properly.
- b. Image resolution should be at least 1-3 megapixels (1280x960 – 2048x1536).
- c. Ensure sufficient environmental lighting. If flash is needed, it is too dark.

- d. Once camera parameters are set, do not change them throughout collection.
- e. Make sure the image series contains significant overlap between photos.
- f. Move the camera positioning with each photo: adjusting the perspective by 10-20 degrees as well as height can improve overall output.
- g. Attempt to maintain a controlled capture environment, with minimal moving objects.
- h. The larger a capture environment, the more images will be needed. There is no limit to the number of pictures VisualSfM will integrate, but processing time will substantially increase.
- i. If there are gaps or holes between the photo perspectives they will have to be filled with additional images to ensure wholesome SfM reconstruction.

#### **3.2.4 Upload and Conversion**

This step of the capture process appears in the complex workflow (see Appendix A). If during the aerial survey wireless connection fails between the GoPro and workstation, the images stored on the camera can be easily uploaded manually. Using either a micro-SD adapter or mini-USB cable the GoPro is able to directly upload all images onto a compatible computer rapidly. Although this manual step detracts from the live-stream advantage used in this project, it may be a necessary step pending a failed wireless connection. Following a successful aerial survey it may be necessary to convert or transform the image series into optimal formats. As mentioned in 3.2.2, certain camera platforms use wide-angle lens that may cause distortion to the image. For most SfM

pipelines it is preferred that input images have as little distortion as possible to best represent accurate depth and shape [38]. There are a few software solutions to correcting image distortion: Adobe Photoshop, DxO, and GIMP. Out of these software options, only GIMP is freeware. Some cameras, such as the GoPro, have high resolution captures settings (12 megapixels) but are only available in wide-lens which causes severe distortion. In this project, the GoPro was set to capture at 7 megapixels to reduce the degree of distortion while sacrificing some image detail. No image conversion is needed when using 7 megapixel medium-lens with the GoPro.

All of the uploaded images on the workstation are now able to be visually reviewed. The image series from the aerial survey must be looked over to determine the quality and applicability of each image. Even though VisualSfM has the ability to deduce image usefulness via algorithm, it is beneficial to quickly review and remove extraneous images. Each image incorporated into VisualSfM increases processing time exponentially, which depending on the total number of images and computing power could translate into a few extra seconds or even minutes to process [54].

### **3.3 Structure from Motion**

#### **3.3.1 Equipment**

The primary equipment in this step is the same workstation used prior (HP Pavilion laptop dv6), hardware specifics and advantages are given in section 3.2.1. This step of the process uses VisualSfM as the structure from motion platform. VisualSfM is an open source platform that employs many cutting-edge SfM algorithms and research tools used in computer vision research. VisualSfM is compatible with the major computer operating

systems (windows, mac, linux), but may require additional support files for proper functionality [56], [57]. The most recent version of VisualSfM is available from the main support webpage: <http://www.di.ens.fr/cmvs>, called version “fix-2”, updated March 27, 2011 [37]. The version “fix-2” updated software package comes equipped with additional functionality such as CMVS, which greatly improve the overall effectiveness of the platform [36]. Installation of the software is clear, but deviations in operating system or computer registry files may require additional steps for complete installation. Full installation documentation can be found at [www.di.ens.fr/cmvs/documentation.html](http://www.di.ens.fr/cmvs/documentation.html). After installation it is beneficial to run the test data tutorial for VisualSfM which comes with the full software package. Performing the tutorial will familiarize the user with the overall interface of VisualSfM and verify program functionality.

### **3.3.2 Setup and Preparation**

Prior to performing any analysis with VisualSfM the working directory and image source folder must be verified. The image series folder created in section 3.2 is the source folder for input images. By default, VisualSfM creates a working folder within the installation directory. Unless there are hard drive space issues or user preference, the default working location for VisualSfM is satisfactory.

VisualSfM has the ability to use GPU in addition to CPU, which potentially accelerates the processing time. Prior to analysis, the performance settings should be maximized to take full advantage of available computer processing power. Within VisualSfM the performance settings can be adjusted from Tools > Enable GPU. Settings

such as ‘set maximum dimension’ and ‘match using CUDA’ are excellent options that improve performance. Settings should be maximized to best suit workstation capacity. The higher performance settings selected, the faster processing occurs, but other computer processes suffer [54]. Once the main SfM steps are initiated, it is best to not interfere with the workstation, allowing full processing power to be dedicated to the SfM task.

VisualSfM has a simple user interface but has the ability to perform complex operations. Although this thesis project only covers the primary uses for the program, there are numerous other capabilities built into the software for other applications. Throughout the remainder of section 3.3, the procedural steps performed in VisualSfM (see Appendix A: Steps A, B, C, D) can be identified on the main UI toolbar (Figure 7) [54].



Figure 7 - VisualSfM Toolbar

This step begins the VisualSfM portion which can be seen in Figure 3 and Appendix A. Opening VisualSfM creates a new project which should be named and saved to the hard drive. The first step in the VisualSfM workflow is loading or importing the image series

(see Appendix A: Step A). Press the ‘Select Multiple Images’ button to initiate the loading prompt (Figure 8).



Figure 8 - Step A

Select all of the desired images for the analysis and import them. The selected images will appear as a thumbnail grid in the VisualSfM UI (Figure 9). From here more images can be added to the series or undesirable images, such as duplicates or blurry, can be removed. Note that while all processes run in VisualSfM a log tracks every action. This log is very useful for monitoring CPU performance and keeping track of processing time or errors in the workflow (Figure 9).

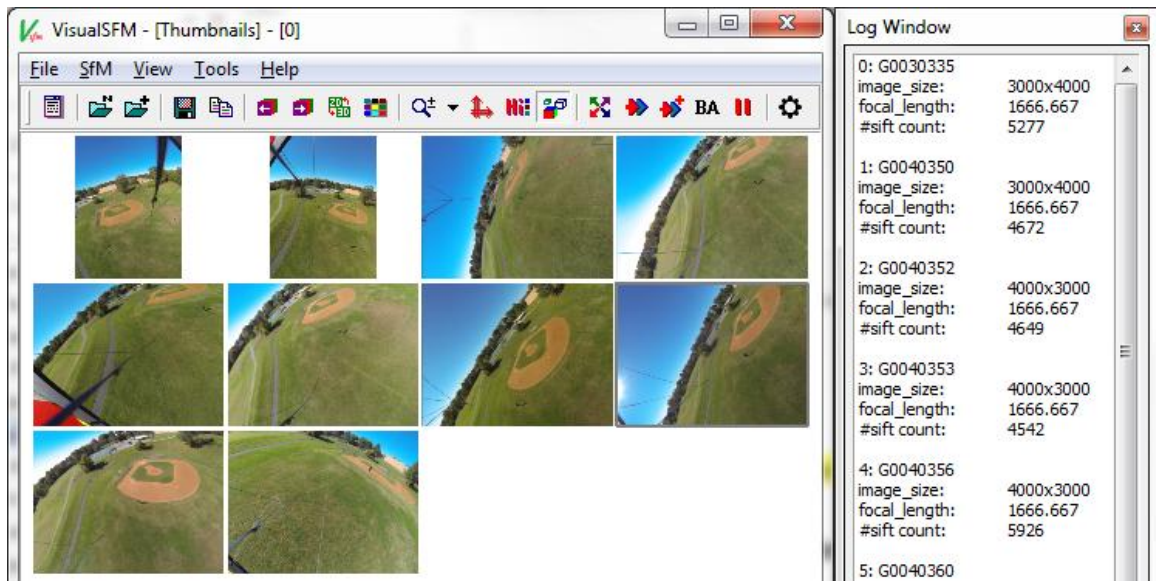


Figure 9 – Image thumbnails and Log

Once the image series is completely loaded into the VisualSfM environment, the workflow can proceed to Step B, SIFT reconstruction.

### 3.3.3 SfM Algorithm

The SfM algorithms used by VisualSfM are a culmination of years of computer vision research developed by Yasutaka Furukawa and Jean Ponce and other research contributors, compiled into the software environment by Changchang Wu [36], [38]–[40]. VisualSfM uses a few steps in the SfM pipeline: SIFT, sparse reconstruction, and dense reconstruction. SIFT is a GPU-accelerated feature detection and bundle adjustment for the SfM system. The SIFT operation systematically analyses all the images within the VisualSfM environment. The result from SIFT creates a metadata file documenting all

identified objects in an image and all similarities between the other images in the series (Figure 10).

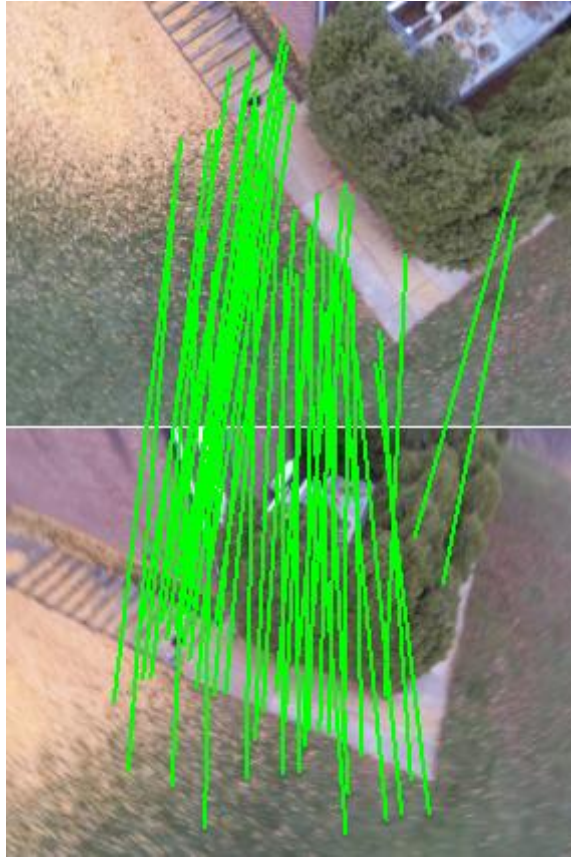


**Figure 10 - VisualSfM: SIFT example**

The second step with VisualSfM is to perform the SIFT operation (Figure 11). This step performs the SIFT operation which identifies the unique features within each image.

Next, the process matches the SIFT features between all the images in the series. The log will track the image SIFTed, the number of unique features detected within the image, processing power dedicated, elapsed time, and number of similar features between each

image pair compared (Figure 11). The amount of processing time required for this step is relatively low, but the number of image comparisons needed will grow exponentially relative to the number of images used in the series. This portion of VisualSfM can take advantage of workstations that have a GPU to accelerate the process. As mentioned earlier in the section, it is preferable to not interfere with the workstation while the SfM procedure is occurring. Fortunately, if the processes during Step B are interrupted for any reason, VisualSfM is able to track the progress of the analyses and resume SIFT and matching where the pipeline ceased.

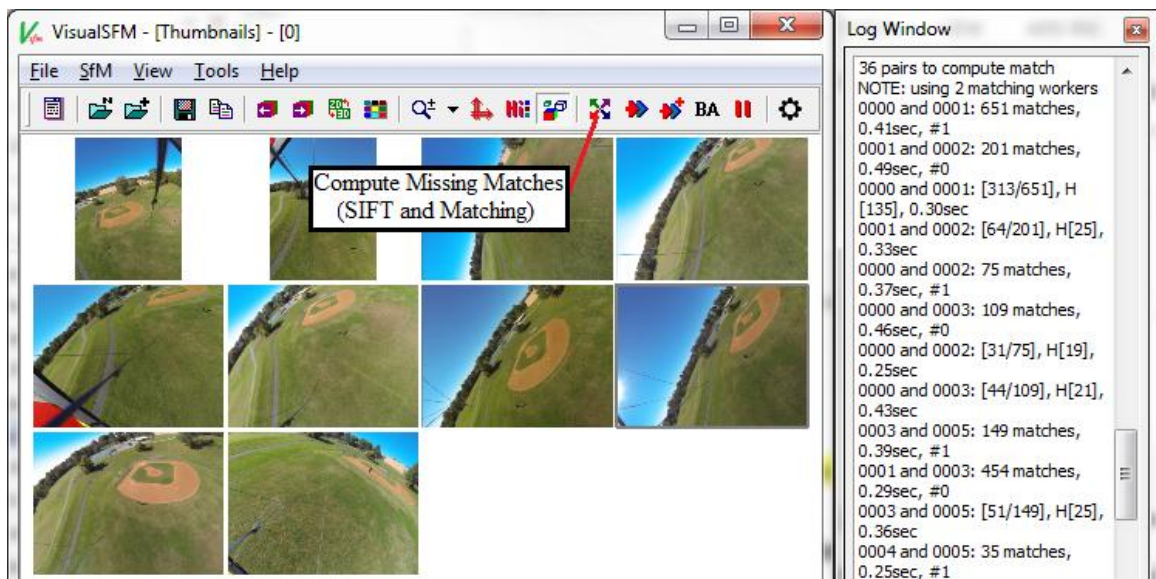


Figure 11 - Step B

The next step with VisualSfM is performing Sparse Reconstruction (see Appendix A: Step C). This procedure in VisualSfM incorporates all previously determined relationships and metadata within each image and the image series and attempts to

construct a rough 3D representation of camera positions and object locations. After Step B is performed, Step C is easily initiated by running ‘Compute 3D Reconstruction’ (Figure 12).



Figure 12 - Step C

During this step VisualSfM systematically displays all of the computed photographs according to their approximate perspective. As each image is added to the display the computed 3D model continues to grow or “solve” (Figure 13). While the program attempts to solve using all the input images the display interface can be navigated, presenting a real-time environment to witness the sparse 3D reconstruction. Sometimes a few separate 3D solves are computed due to inadequate overlap between the images in the series. These separate solved models will appear in the log window along with the images used to create them. If rogue image solves occur that are separate from the primary model, additional photos may have to be captured or manual relationships defined to patch the gap. Another option is to remove the images that are causing confusion for the 3D reconstruction. There are two methods for removing unwanted images from solved models [54].

Method 1:

1. Turn off 3+
2. Press F2 – select bad 3D points
3. Click “” icon twice – deletes camera with the most points selected
4. Repeat from step 1 if bad points remain
5. Click “” to grow the modified model

Method 2:

1. Press F1 – draw rectangle to select bad cameras (250 camera maximum)
2. Click “” icon to remove all selected bad cameras
3. Click “” to grow the modified model

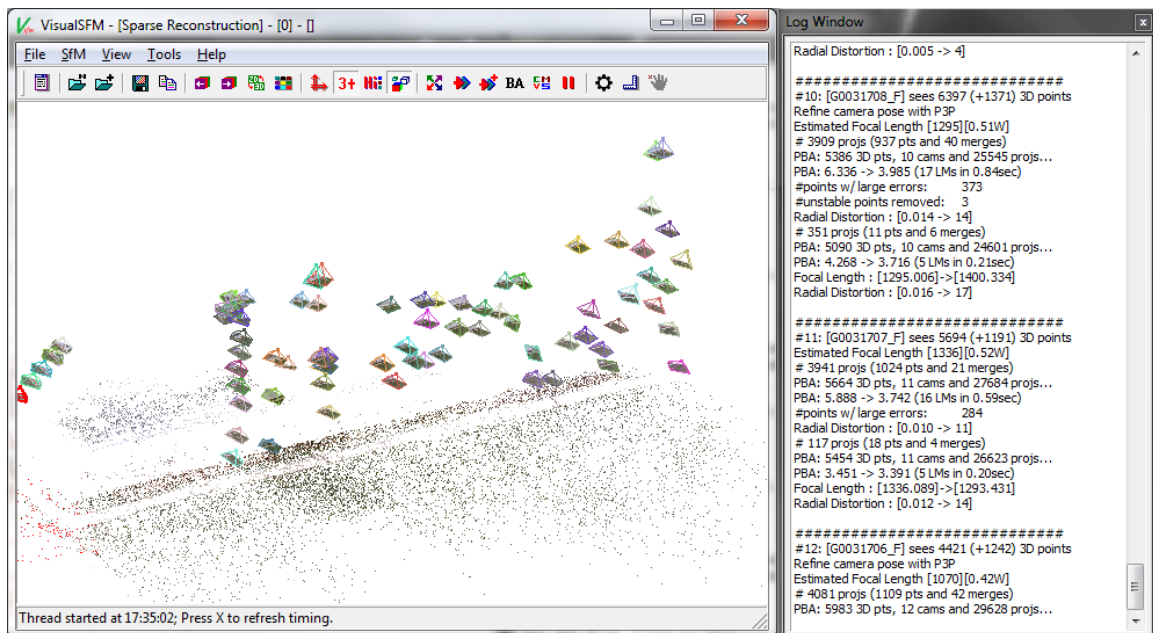


Figure 13 – Step C: VisualSfM Sparse Reconstruction

The final output of the computed sparse 3D reconstruction is the best-estimate position of all the input camera perspectives and a sparse point cloud of the object similarities between all the images. This constructed environment can be navigated in the display UI and checked for integrity.

The final step using VisualSfM is creating the dense reconstruction (see Appendix A: Step D). This operation is only available from the toolbar if the previous step C has completed successfully. The dense reconstruction process uses the sparse 3D reconstruction as a foundational benchmark and improves the point cloud density by identifying additional features within the image series [36]. The operation is initiated by selecting the “Compute Dense 3D Reconstruction using CMVS/PMVS” button from the toolbar (Figure 14).



**Figure 14 - Step D**

Beginning the dense reconstruction procedure activates a dialog to create a working folder to save the resulting files and computations. Once again the folder name and location are arbitrary as long as they can be located for future application. Step D creates numerous output files that reference different aspects of the dense reconstruction. The

three output files that are of most concern for this project are: *bundle.rd.out*, *list.txt*, and *NamedDenseCloud.ply*. Having created the working folder for CMVS, VisualSfM commences the dense reconstruction algorithms. This step requires more computing power than StepB or C, and will not visually display the results as it progresses. The log will continue to update CMVS status as each stage of the analyses proceeds (Figure 15). Once completed, the dense reconstruction results from CMVS can be viewed in the UI display by activating “View > Dense 3D Points”. The result displayed in the UI represents all of the estimated camera perspectives along with a more dense view of object points identified within the image series (Figure 15).

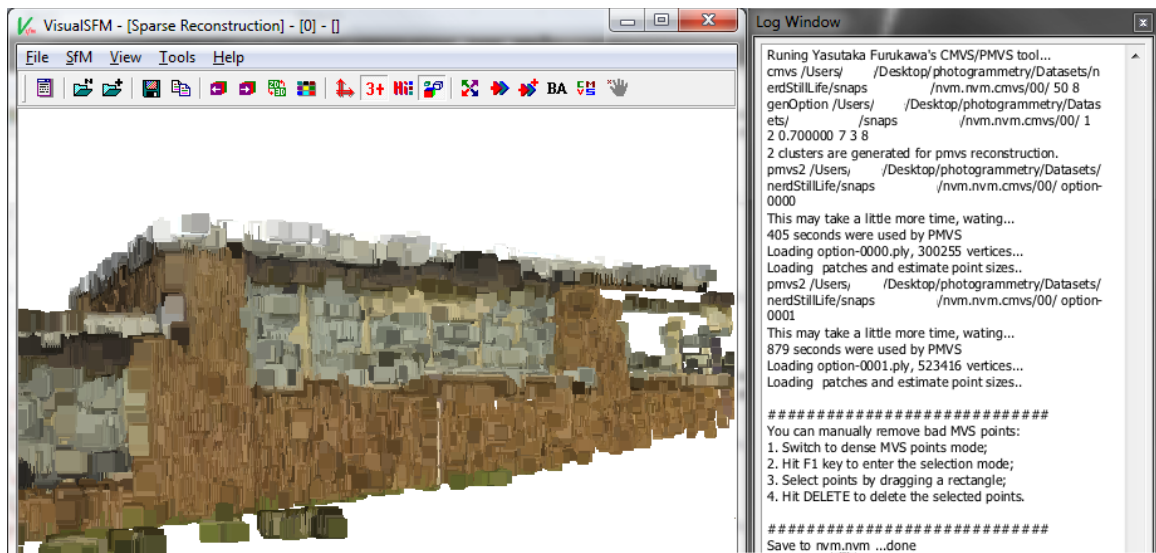


Figure 15 - Dense point cloud

### 3.3.4 Point Cloud Export

It is important to note that all features established as matching between the images are represented as points within the display UI. Step C resulted in a sparse point cloud,

effectively showing the prominent features that at least 3 cameras similarly agreed upon. Step D applied algorithms that progressed deeper into each image and identified additional features and similarities, creating a denser point cloud. The output files created from Step D (*bundle.rd.out*, *list.txt*, *NamedDenseCloud.ply*) are automatically compiled within the working folder established before the process runs. *Bundle.rd.out* is considered a project file type and contains imbedded information about the sparse point cloud and the images used during 3D reconstruction. *List.txt* contains the camera perspective information which is used for projecting the texture over the 3D mesh. *NamedDenseCloud.ply* is the dense 3D reconstruction result from CMVS and contains the dense point cloud output from Step D. Following a successful completion of Steps A-D, the three output files from VisualSfM are prepared for further 3D reconstruction in MeshLab.

### **3.4 3D Reconstruction**

Following the established workflow the output point cloud from VisualSfM is imported into MeshLab for 3D reconstruction (see Appendix A: Step E). MeshLab is the primary open source program utilized in this study for 3D model reconstruction. MeshLab is a widely accepted open source platform for manipulating 3D environments, models, and point clouds [2], [26]. The platform contains a large community of developers and contributors who continually improve and add plug-ins. Most of the built-in functions available in MeshLab for 3D reconstruction are considered the ideal approach, such as Poisson's Surface reconstruction [43], [45]. MeshLab is commonly used for preliminary

3D data optimization and cleaning, but also contains the ability to produce and finalize 3D models with high-resolution photo-realistic textures.

### **3.4.1 Equipment**

The primary equipment in this step is the same workstation used prior (HP Pavilion laptop dv6), hardware specifics and advantages are given in section 3.2.1. This step of the process uses MeshLab as the 3D reconstruction platform. MeshLab is an open source platform that employs many current rendering and manipulation tools used in 3D modeling [26]. A brief list of MeshLab capabilities include: editing, cleaning, healing, inspecting, rendering, and converting 3D meshes [26]. The program also has a diverse compatibility library, being able to import and manage at least 18 major data types and file extensions. The MeshLab program began in 2005 within the computer science department of University of Pisa, developed mostly by students. The platform continues to receive technical support and upgrades, the most recent update of MeshLab version 1.3.3 was released in April 2014. The software is available on all major operating systems (windows, mac, linux), but known installation problems exist. Full installation documents for each operating system can be found on the main MeshLab website: <http://MeshLab.sourceforge.net> [26]. There are test datasets installed along with MeshLab that are available for tutorial. Performing the tutorial will familiarize the user with the overall interface of MeshLab and verify program functionality.

### 3.4.2 Setup and Planning

MeshLab is a well-designed open source program providing complex, advanced 3D techniques with a simple to install-and-use interface. The amount of processing demanded by the program is directly related to the size (mb/gb) of the dataset it is managing. MeshLab has the capacity to handle millions of points and thousands of polygonal mesh faces, which is more numerous than the datasets tested and used in this project. The toolbar available in the program UI contains the most frequently used functions for basic rendering and navigation (Figure 16). There are hundreds of additional functions and algorithms built into MeshLab accessible through the “Filters” and “Render” menus.

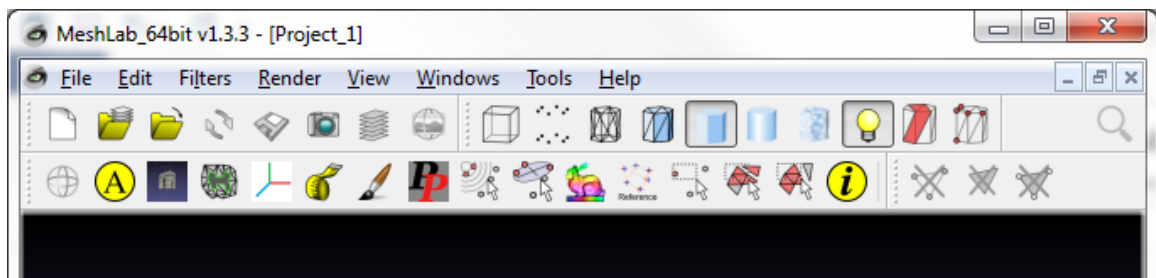


Figure 16 - MeshLab Toolbar

The first step (Step E) using MeshLab begins with loading the output project created in Step D, section 3.3.4 (see Appendix A: Step E). This step is straight-forward because MeshLab has the built-in functionality to read and load the file types created from VisualSfM dense reconstructions. Select the “Open Project” button and navigate to the *bundle.rd.out* file created in step 3.3.4. Once this file is located and selected MeshLab will also prompt for the related camera file, *list.txt*, which is then selected. The data will

only take a few moments to load into the program environment. Loading all of the files should have also opened the Layer Dialog window. If this window is not visible, activate it through selecting View > Show Layer Dialog (Ctrl+L). In addition to displaying the 3D point cloud, the Layer Dialog window also includes all of the images used during the creation of the point cloud in VisualSfM. At this time a point cloud is visible in the main display window and the two data windows on the side of the UI contain the point cloud layer (called a “mesh” in MeahLab) and all the image files (Figure 17).

Prior to beginning the next step, navigate around the main display to inspect the point cloud integrity. The images in the Layer Dialog can also be selected which will reposition the user perspective to that of the selected camera. The size of the camera views and point cloud vertices can be adjusted for improved visibility.

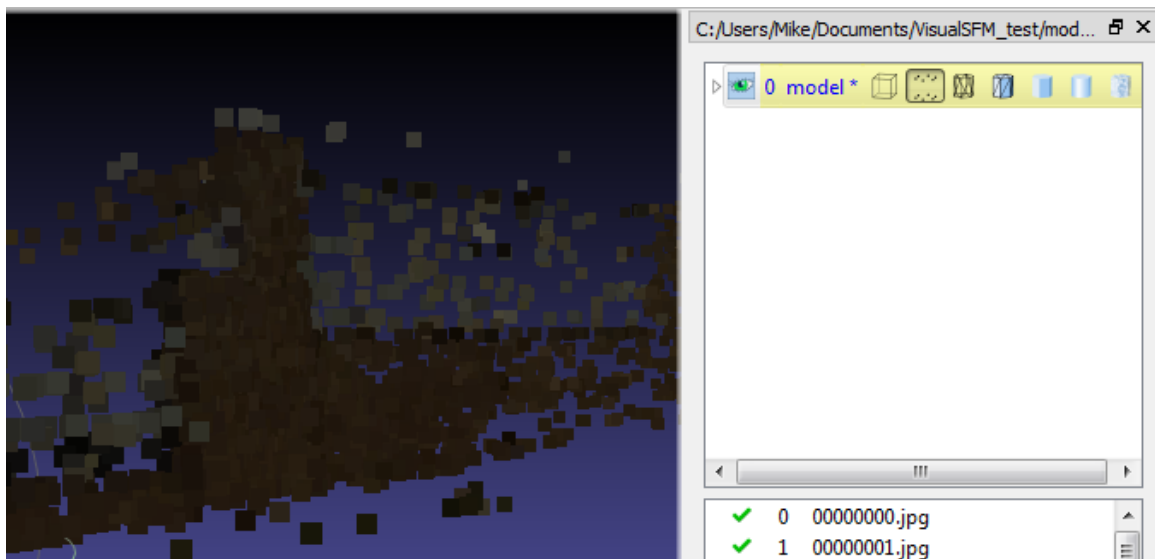


Figure 17 - MeshLab UI

Following the successful loading of the project, the dense point cloud produced in section 3.3.4 is swapped into the project, replacing the sparse point cloud (see Appendix A: Step F). This step is needed because the project file *bundle.rd.out* only contains the sparse point cloud and camera positions. By switching to the dense point cloud MeshLab is able to retain the proper camera positions and image textures for later application on a much higher fidelity 3D mesh. First the current “mesh” (sparse point cloud) must be removed, which is done by right-clicking the model in the Layer Dialog and selecting “delete current mesh”. All that remains in MeshLab are the images and corresponding camera positions. Then select File > Import Mesh, selecting the *NamedDenseCloud.ply* model file from the output working folder from 3.3.4. Executed correctly, this step presents the much higher density point cloud produced by the CMVS algorithm in VisualSfM (Figure 18). Similar to above, use the display UI to navigate around the 3D scene and identify visual continuity.



**Figure 18 - MeshLab: Dense point cloud**

The next step involves cleaning the dense point cloud dataset of extraneous or unwanted points, which is necessary for improving 3D mesh reconstruction using Poisson's algorithm (see Appendix A: Step G). A drawback is that this step requires actual user manipulation of the point cloud dataset. Due to scene interpretation and possible user error, it is best to have a user that is familiar with the scene and data collected. Not all bad points need to be cleaned at this time. This cleaning procedure can be applied progressively as Poisson's mesh is created and adjusted in the subsequent section. To select unwanted vertices select the “” button on the toolbar. Highlight the bad vertices that are far from the scene center or visibly incorrect according to the knowledge of the AOI. By holding Ctrl or Shift on the keyboard while highlighting vertices, groupings of vertices can be added or remove from the selection. With a collection of vertices selected, pressing the “” button will delete them from the MeshLab dataset. It

is important to note that the vertices will not be deleted from the original

*NamedDenseCloud.ply* file, which allows room for trial-and-error. Once the point cloud is cleaned to satisfaction it can be analyzed by the 3D surface reconstruction algorithm.

### 3.4.3 Algorithm Application

Applying the Poisson's surface reconstruction algorithm is a simple step, but contains many possible variables (see Appendix A: Step H). Due to the many outcomes that can emerge from the Poisson variables, this step is highly adjustable and must be approached precisely. Poisson's surface reconstruction is initiated by selecting Filter > Points > Surface Reconstruction: Poisson. Activating Poisson's reconstruction prompts the user for 4 input variables to adjust the output mesh: Octree depth, Solver divide, Samples per node, and Surface offsetting (Figure 19).

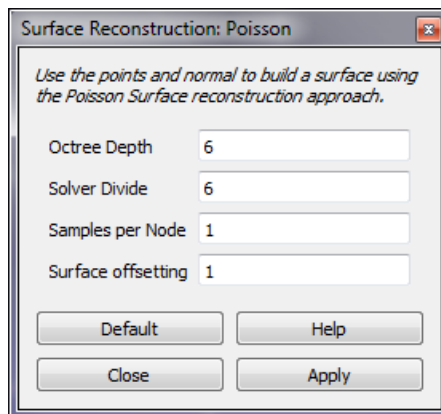
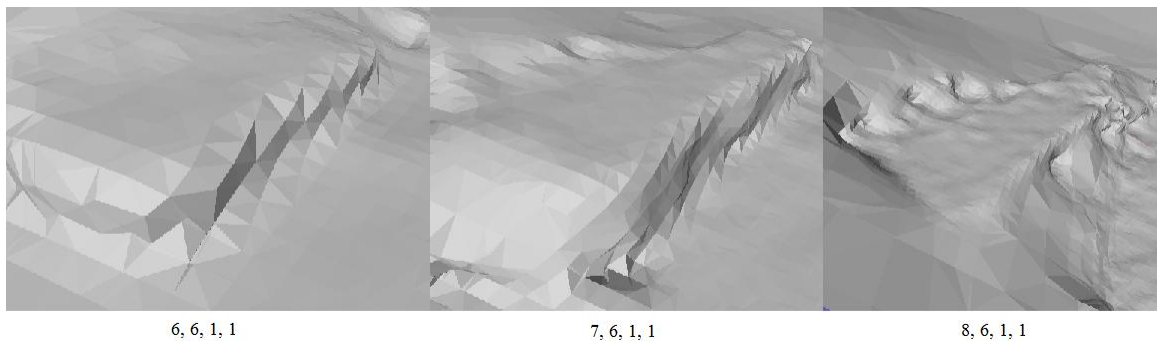


Figure 19 - MeshLab Poisson's parameters

Each of these variables slightly alter the algorithm for building the 3D mesh. For a much more detailed explanation of the variables, refer to the original document from the developers of the Poisson's reconstruction [45]. In short, the octree depth has the most significant control over the detail of the mesh. The higher the parameter number becomes, the more detailed the result will be in relation to the point cloud, but with a cost of processing speed (Figure 20). The samples per node parameter defines how many points the algorithm puts into one node of the resulting octree. If the point cloud is rough or noisy a high sample per node value will smooth the mesh result, while a low value will retain model detail (Figure 20). Beginning with the default parameter values will establish a baseline for the numerous iterations of Poisson's surface reconstruction.



**Figure 20 - Poisson results**

Step H may require multiple iterations of Poisson's surface construction before producing a mesh result that is satisfactory to the user. A degree of trial-and-error with Poisson parameters will occur before an optimal mesh emerges. Even with a satisfactory Poisson mesh some edge cleaning will be required.

Step I addresses the final steps of cleaning the Poisson mesh before textures are applied (see Appendix A: Step I). The primary objects being corrected in this step are non-manifold edges, which are defined as geometry where any edge is shared by more than two faces. Some algorithms are unable to process geometry that have non-manifold edges, such as the texture application in the next step. This requirement for manifold edges may be considered a drawback for MeshLab, creating an extra step in the procedure and potential empty holes in the 3D mesh. Non-manifold edges are fixed by selecting Filters > Selection > Select Non-Manifold edges > Apply, then deleting them with the appropriate feature delete button. Additionally, the mesh is prepared for texture application by parameterizing between the input images and the projected faces of the mesh. This process re-matches the images and identifies the best camera perspective for each face of the mesh. Parameterization is initiated by selecting Filter > Texture > Parameterization from registered rasters. Best results have been found from selecting boxes 1, 2, 4, and entering “4” into Texture gutter (Figure 21).

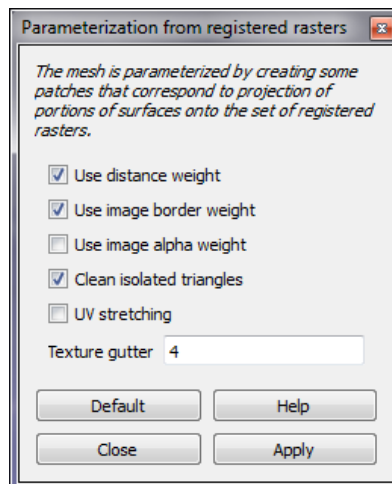


**Figure 21 - MeshLab Parameterization**

### 3.4.4 Texture Application

Applying the visual texture to the final Poisson mesh is a simple and satisfying step in MeshLab (see Appendix A: Step J). Due to the preparations in previous steps, draping the imagery on the 3D mesh is quick. Using parameterization from Step I allows the best-fit images to be used for each model face. Projecting the textures onto the model is initiated by selecting Filters > Texture > Project active rasters color to current mesh, filling the texture, using basic weighting. There are a few parameters that need to be defined for this step. The texture file is the given name of the texture that is created from this process. Pixel size is any power of 2, but usually within the boundaries of the image resolution; there is no limit to the size of the texture resolutions e.g. 512, 1024, 2048, and 4096. The remaining parameters can be selected by the user, but recommended settings are shown below (Figure 22).

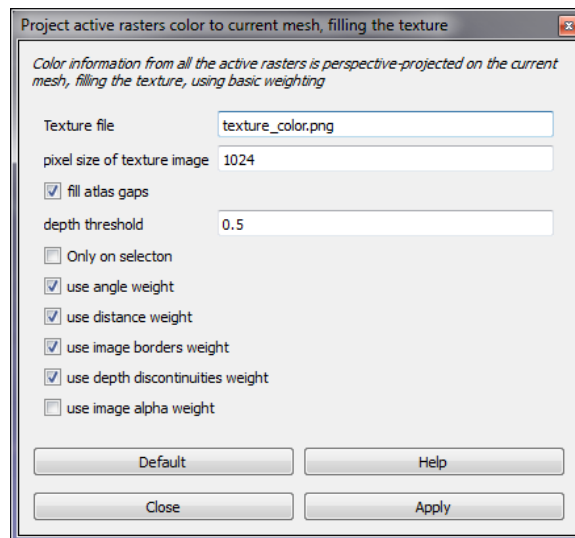
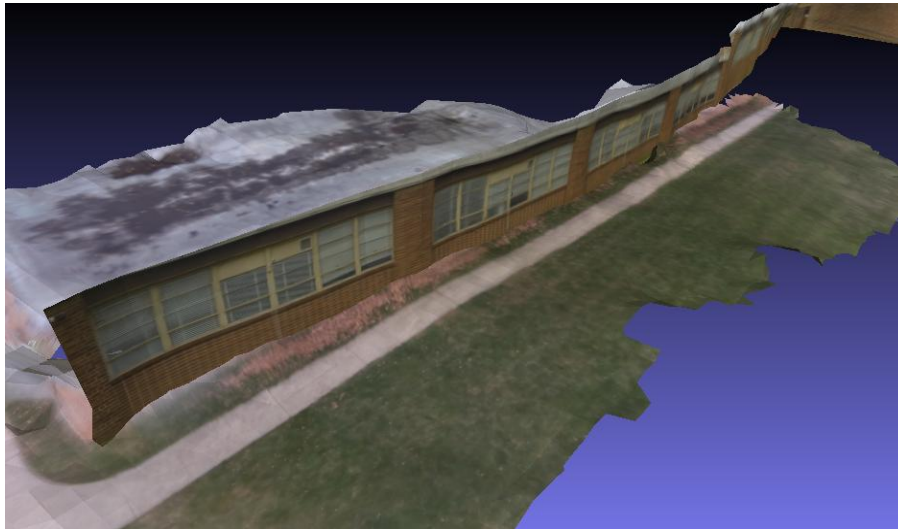


Figure 22 - MeshLab Project Texture

Once applied, the image textures appear draped over the 3D reconstructed surface mesh.

Applying the textures to a model surface creates a significantly improved visual product.



**Figure 23 - Final Model with Texture**

## CHAPTER FOUR: RESULTS

This chapter of the thesis summarizes the results from the project working demonstration performed at the proposed AOI using the methods outlined in chapter 3. Each following section reviews the input and results from each stage of the workflow.

### 4.1 Overview

The final field survey captured 162 usable images and totaled 80 minutes to produce the final 3D scene reconstruction from the time of the survey. The sparse point cloud was created in 30 minutes within VisualSfM, which is a recognizable point model of the scene, and could be easily used for rapid analysis or guidelines for manual feature extrapolation. The elapsed-time for the entire workflow beginning from arrival at the AOI is documented in the table below (Table 1).

Table 1 - Workflow time

Step	Description	Time (min)
Equipment	Boot and sync workstation and camera	5*
Survey	Commence aerial survey and data capture	10 – 40*
Transfer	Transfer images from camera to workstation	5
Step A	Load and clean image series in VisualSfM	3
Step B	Perform SIFT and image matching	20
Step C	Sparse 3D reconstruction (point cloud)	7

Step D	Dense 3D reconstruction (point cloud)	30
Steps E-F	Load SfM project into MeshLab	5
Step G	Clean bad points in cloud	5
Step H	Execute Poisson surface reconstruction	5
Step I	Clean bad faces in reconstructed 3D mesh	5
Step J	Create and project texture onto 3D model	1 - 4
Step K	Export final 3D model for analysis or	1
	<i>*equipment set-up and survey not included</i>	<hr/> ~80 min

Using fewer images throughout the workflow would significantly reduce the overall time, with 50 images taking about 15 minutes for a sparse point cloud and 45 minutes for the final 3D model. The same 162 images were uploaded into Photosynth to compare processing speed for the sparse point cloud, which Photosynth is capable of producing. Uploading the images, performing its proprietary algorithm, and producing the final visible result totaled about 25 minutes in Photosynth, 5 minutes faster than the method used in this project. On the other hand, Photosynth requires an internet connection to upload the images and then perform SfM. Processing the captured images with Photosynth in the field would only be possible with a cell card installed in the workstation, which is neither fast nor reliable. Also, the point cloud result Photosynth produced was only created from 105 images of the 162 uploaded (65%). Through Photosynth's automated process, it lost over one-third of the image data captured during the survey. 123D Catch was unable to process the images due to its limitation of only 70 images.

The total cost of the research project, including equipment already owned (workstation, kite) totaled \$835. This cost is substantially lower than many research groups, response teams, and companies expect to spend when attempting their own surveying and 3D data acquisition [2], [8], [21]. Any individual item used in this project is able to be upgraded or substituted for another comparable item. A list of cost breakdown is shown below.

**Table 2 - Project Costs**

<b>Item</b>	<b>Description</b>	<b>Cost (\$)</b>
Workstation	HP Pavilion dv6	500.00
Camera	GoPro Hero 3 Black	250.00
Aerial platform	Performance kite	50.00
SfM software	VisualSfM, Bundler	0.00
3D software	MeshLab	0.00
Assorted gear	String, harness, etc.	5.00
Transportation	Travel to survey AOI	30.00
		<b>\$835.00</b>

## **4.2 Data**

A total of five survey sessions occurred at the AOI over the duration of the thesis research project (Figure 1). The final two surveys incorporated the complete refined workflow developed during the earlier phases of the project. The final survey presented the best weather conditions as well as images results. A total of 320 photographs were captured by the GoPro during the final survey. During the aerial capture session the

wireless link between the workstation and camera was maintained and the images were able to successfully transfer. Total aerial surveying time did not exceed 40 minutes.

Additional surveying did not occur due to the completeness of the final image series, but performing another survey at that time could have easily occurred. Due to the maintained wireless link, the imagery was immediately accessible on the workstation for manual integrity review. Out of the 320 photographs captured during the field survey session, 162 were identified as useable.

The estimated average altitude of the kite was around 70 feet, with the maximum oblique camera angle calculated to around 40-45°. The extent of the AOI captured by the camera in a single image from an altitude of 70 feet is represented in the figure below (Figure 24). Majority of the images were captured with angles lower than the maximum or nadir. The visible extent of the kite is useful in determining what objects in the scene will be better surveyed. Objects closer to the sensor will experience a greater degree of perspective change, therefore more easily calculated and recognized by SfM algorithms. Especially with more oblique images, the objects above the focal horizon will become less useful for SfM calculations due to their minimal perspective movement.



**Figure 24 - Camera view from 70 feet altitude**

With an oblique camera angle of  $45^\circ$  and a kite altitude of 70 feet, the estimated useful viewing distance for SfM is less than 100 feet measured from the ground position of the sensor, with the field of view limited by the camera lens. The disadvantage of oblique imagery can be overcome with additional perspectives from the camera. The more angles available to the SfM algorithm, the higher possibility it has to calculate feature position within the AOI.

The data captured and used throughout the thesis project is summarized below (Table 3). The foundational data required for the success of the project workflow is the aerial imagery. Depending on the camera platform and aerial vehicle used for surveying, the quantity and quality of images will differ. In total 162 images of the surveyed AOI are used in the 3D reconstruction workflow. The satellite imagery and GIS vector dataset are used within a GIS for verifying the data accuracy and integrity.

**Table 3 - Data Table**

<b>Data type</b>	<b>Measurement</b>	<b>Source</b>
Oblique/Nadir aerial photography	100 pictures used 122 mb total 5 Megapixel	GoPro Hero 3
Ground level photos	62 pictures used 119 mb total 5-12 Megapixel	GoPro Hero 3 Canon Digital
Nadir aerial/satellite imagery	X mb - streamed	Google, GeoEye, Digital Globe
GIS vector dataset of GMU campus	437 kb	GMU GGS department

### **4.3 Structure from Motion**

Multiple sessions of workflow processing occurred to test the integrity of the pipeline in different settings and with varying datasets. Prior to field application of the refined workflow in phase 3 of the project (see Appendix B), test image datasets were used to formulate the optimal SfM and 3D reconstruction steps. These steps were refined and developed through phase 1 and 2 of the project (see Appendix B). The following section summarizes the input data, variables, parameters, and results of the SfM workflow performed during the final field test. A detailed procedural workflow of these steps are found in chapter 3 and summarized in Appendix A.

**Step A:** Within VisualSfM, the 162 selected images from the final survey are loaded into the program using “Open Multiple Images”. Loading takes a fraction of a second per

image, with the whole image series taking about 3 minutes. The image series is visible as a 2D grid within the UI display (Figure 25).

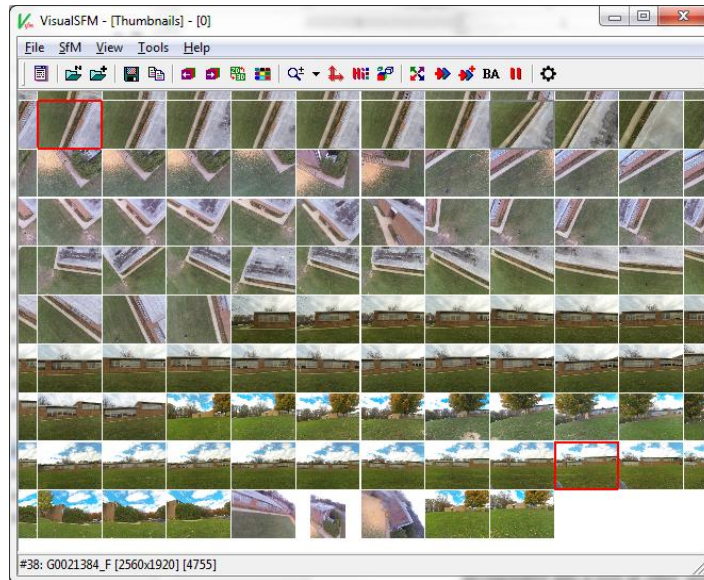


**Figure 25 - Results: Step A**

**Step B:** Once loaded, the images must be analyzed for features and similar matches. This step is initialized by pressing the “Compute Missing Matches” button. This step is CPU processing heavy and the workstation is not interfered with. In total the SIFT operation and matching takes roughly 20 minutes. The result of this step is not immediately visible, but the image matching and relationships calculated from the SIFT operation can be plotted for visual representation (Figure 26). These graphs display the hierarchal relationship between the images (spanning tree) and number of similar features (match matrix).

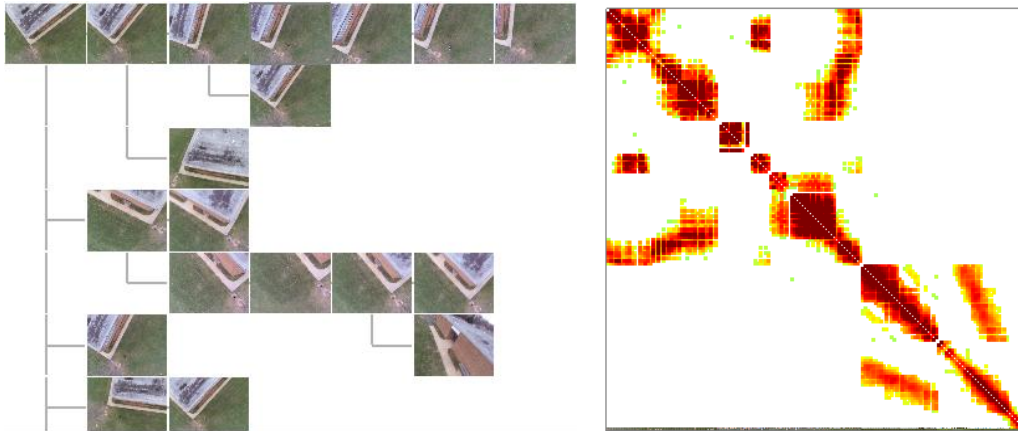


**Figure 26 - Results: Spanning tree and Match matrix**

Following this step there were three images identified without significant matching pairs, therefore excluded from the graphs and future analyses. Further investigation determined that the perspective from the three excluded images was vastly different from the remaining group, and the workflow should continue without them.

**Step C:** Sparse reconstruction only become available as an option within VisualSfM once an image series with computed matches is loaded. This step is initialized by pressing the “Compute 3D Reconstruction” button on the toolbar. While the program systematically displays the camera perspectives the 3D point cloud progressively grows in complexity (Figure 27). During this step the display UI is navigable by the user.

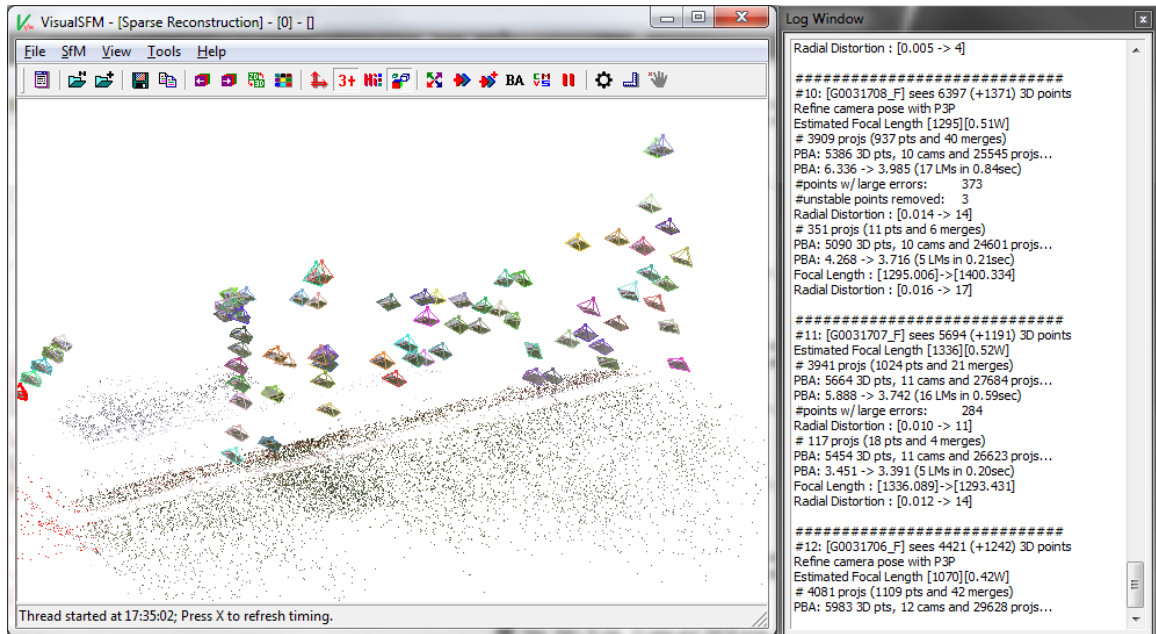


**Figure 27 - Results: Step C**

Full sparse cloud reconstruction of all the images takes about 7 minutes. During this step three model iterations were built, each one becoming progressively more intricate, eventually producing the final sparse point cloud. No additional images were identified as poor matches or were unable to be projected into the point cloud.

**Step D:** With the sparse point cloud completed, the dense point cloud can then be calculated. Dense 3D reconstruction utilizes the CMVS procedure, which is initialized by pressing the “Run Dense Reconstruction” button on the toolbar. This step requires significant CPU processing as well and should not be interfered with. Once started, the dense 3D cloud reconstruction takes about 30 minutes. The final result is viewed in the display UI by selecting View > Dense 3D points (Figure 28).

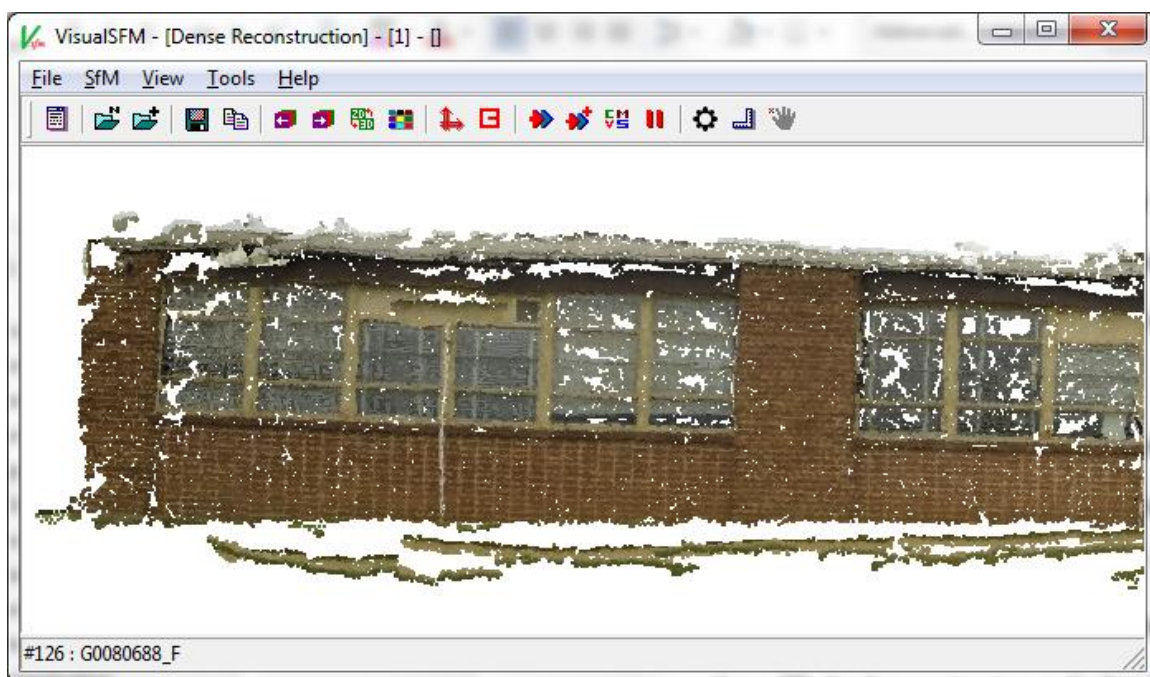


**Figure 28 - Results: Dense Point Cloud**

The dense 3D reconstruction step simultaneously creates a unique working folder for the dense point cloud model. Within the folder are the three main files that are used in the following step: *bundle.rd.out*, *list.txt* and *model\_1.ply*. The remaining steps are performed in MeshLab.

#### **4.4 3D Reconstruction**

**Step E and F:** These two steps are very brief and involve similar procedures to accomplish. In MeshLab the *bundle.rd.out* project is opened by selecting “Open Project” and navigating to the saved directory. After the project file is selected the camera file is requested, which is the *list.txt* file inside the *bundle.rd.out* project. At this time all images used to produce the point cloud and the sparse point cloud are present in the MeshLab

display. Without manipulating anything, the point cloud mesh is deleted. The dense point cloud replaces the sparse point cloud by going to File > Import Mesh, and selecting the named .ply file, in this case “model\_1.ply” (Figure 29). These steps take less than 1 minute in total. The imported dense point cloud then must be cleaned for proper Poisson reconstruction execution.

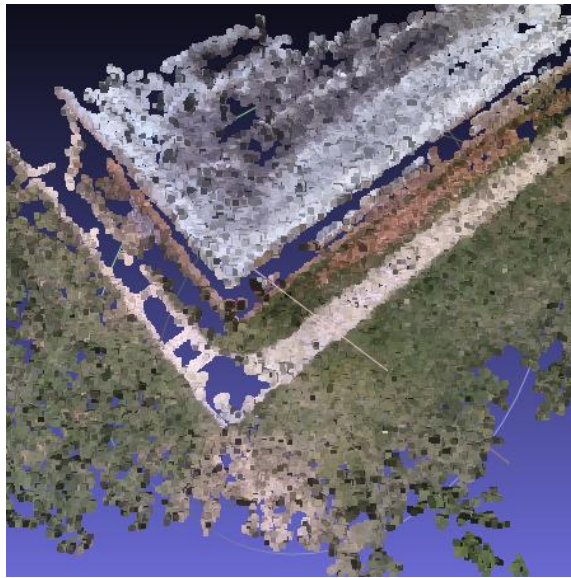


**Figure 29 - Results: Dense Point Cloud 2**

**Step G:** Cleaning the erroneous points in the dense point cloud is simple but potentially flawed due to user interpretation. Extra care is taken to ensure the overall point cloud integrity is maintained while the loose points are removed from the dataset. This step takes around 5 minutes to complete.

**Steps H and I:** Poisson’s surface reconstruction is a particular procedure, yet is considered one of the best point-to-surface reconstruction algorithms in computer vision.

Numerous iterations of the algorithm were applied using varying parameters. The ideal Poisson mesh for this instance was created using octree depth – 7, solver divide – 6, and the remaining values of 1. The resulting mesh is relatively accurate compared to the point cloud (Figure 30).

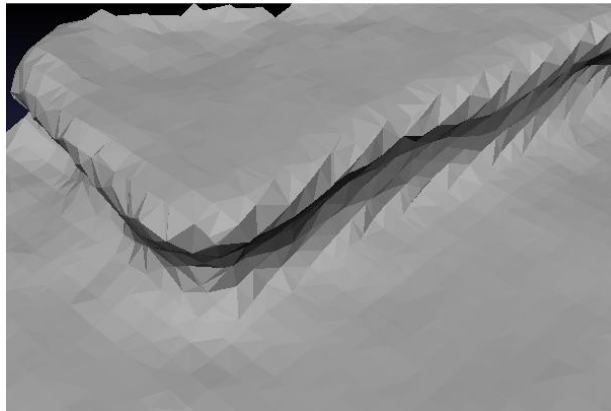


**Figure 30 - Results: Steps H, I**

With a satisfactory Poisson mesh layer, further cleaning commences to better represent the surveyed AOI (Step I). Using similar selection and removing techniques as with the erroneous vertices in the point cloud, the improper mesh faces are deleted from the model. This portion of the step is dependent on the user familiarity with the scene and amount of discretion used to delete or retain areas of the AOI. Non-manifold edges were removed using the select features process described above. The 3D model is then prepared for texture application (Figure 30). Producing the preferred Poisson 3D surface model and cleaning the mesh totaled around 5 minutes.

**Step J:** Using MeshLab is advantageous for applying image textures to models because the imported project from VisualSfM has the camera angles and rasters included with the point cloud. With the cleaned 3D scene model ready, the corresponding images are parameterized against the 3D mesh, recalculating the optimal image to use for each face of the mesh. Two separate texture files were created with different pixel size values: 1024 and 2048. The 1024 pixels size produced acceptable texture results with slight blurring and lack of detail, taking less than a minute to process (Figure 31). The 2048 pixel size produced incredibly detailed textures with spatial resolution equal to the input images, taking about 4 minutes to process (Figure 31). Depending on the speed and quality of the desired texture, this step is variable. For the final model texture, the 2048 pixel size texture layer was used (Figure 23).



**Figure 31 - Step J: Textures**

**Step K:** The 3D reconstructed model completed via SfM from aerial imagery is then prepared for analysis and application (Figure 23). The textured models in MeshLab must be exported as the desired file type. In order to ensure the texture is included with the 3D model it is exported as a “.ply” file. This 3D file type is very common and is accessible by almost all 3D rendering and GIS platforms.

#### **4.5 Accuracy Comparison**

This section of the chapter compares the relative accuracy of the produced 3D dataset from the thesis workflow against other available data, a CAD dataset with building footprints of GMU campus. The relative applicability of this thesis workflow is also compared against the uses for 3D reconstructed scenes within other relevant fields.

In order to test the accuracy of the output datasets, the 3D sparse point cloud and final texture model are compared with CAD building footprints within a GIS. The 3D datasets created in MeshLab have the ability to be geospatially rectified by using the reference tool. Providing four real-world coordinates as control points, the models are able to be adjusted to match coordinate systems (Figure 32). Once the 3D model datasets are scaled and rectified using four control points, the RMS errors of the models are under 0.2 meters. It is possible to add more control points and receive a more accurate transformation, but more precise control points need to be determined.

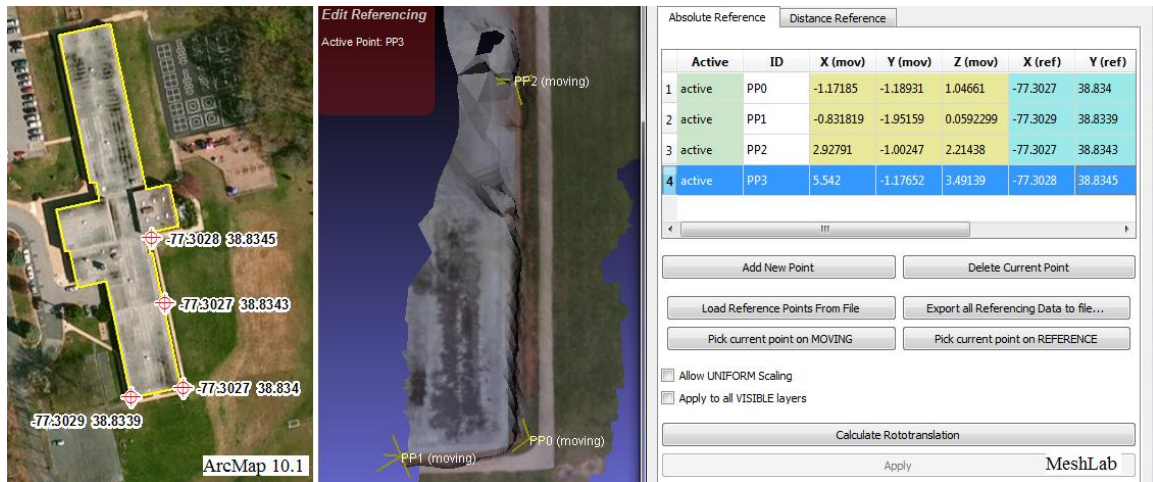


**Figure 32 - Georeferencing Model**

Overlaying the 3D sparse point cloud and the final 3D texture model onto GMU building footprint shapefile in GIS produces promising accuracy results. The overall distortion experienced by the model according to the input ground control points is under 0.2 meters. This value is relatively low by survey standards and could be improved even more. The input control points were estimations taken from satellite imagery on Google Maps, which has a stated horizontal accuracy of up to 6.1 meters. These values could be vastly improved by using precision GPS or theodolite surveying equipment. Assessing the relative accuracy of the output 3D models is performed after geospatial rectification. Due to the SIFT algorithms performed during SfM, each image is precisely placed in relative space to each other [41]. These equations ensure that provided undistorted imagery, the relative position of objects and features within the image series are exactly precise, only limited by the pixel resolution of the input images. This precise quality is present in the 3D models produced. Measuring relatively, the models present excellent

accuracy, down to the relative size of bricks and even space between window blinds (Figure 31). The 3D sparse point cloud also provides incredibly accurate measurements of the identified significant features, such as building edges, corners, and light objects. Even if the 3D models were unable to be geospatially rectified, knowing the measurement of a single feature within the scene could provide a scale to establish relative dimensions for the entire scene.

Four datasets are produced from the thesis workflow that can be used in research and application: image series of AOI, sparse 3D point cloud, digital elevation model (DEM), and final 3D model. Each dataset has potential applications within related fields of research and industry.

**Table 4 - Output datasets**

<b>Dataset</b>	<b>Format</b>	<b>Process time</b>
Aerial survey image series	JPG, TIF, PNG	Instantly during or immediately following survey
Sparse 3D point cloud	PLY, OBJ	10-30 minutes following survey depending on image count
Digital elevation model	Raster formats	10-30 minutes following survey depending on image count
Final textured 3D model	PLY, OBJ	30-80 minutes following survey depending on image count

The image series captured during the survey is immediately available for review. Having an aerial view of a scene can provide near real-time information and data about a

situation. Also, having aerial imagery offers perspectives that are otherwise not possible from ground vantage points. In addition to immediate viewing, aerial imagery can be overlain on topographic maps and elevation data to enhance spatial detail. The sparse 3D point cloud created in step C quickly delivers (10-30 min) a partial 3D representation of the AOI that can be interpreted by analysts. Having a generalized representation of a scene can be almost as useful as a full model when an area only has to be simply mapped. Most 3D sparse point clouds produced from SfM have identified all the significant features and object within each image and interpreted that information into the vertices. Even with minimal spatial training users and analysts alike can deduce the objects within a 3D sparse point cloud. For a geospatial data production pipeline, the 3D sparse point cloud provides more than adequate detail about features in the AOI for geospatial units to be extracted. For instance, the extent and edges of the Green Acres building surveyed in this project were thoroughly visible within the sparse point cloud (Figure 13). An analyst could easily capture a representative building polygon or create an accurate 3D building model based on the point cloud information. Although not produced within the presented workflow, a DEM can easily be extrapolated from both the sparse or dense 3D point clouds. DEMs are commonly used as the topographic foundation for areas of interest and provide precise elevation information about ground and surface features. An accurate DEM can be produced within MeshLab after additional cleaning by exporting either the point cloud layer or 3D Poisson surface as compatible raster layer or 3D polygon file types. The final textured 3D model produced by the thesis workflow delivers a complete product for visual modeling and spatial analysis. The model incorporates high-resolution

imagery from the aerial survey, spatial accuracy and framework from the SfM point clouds, and visual cohesiveness of Poisson's mesh to create a final scene ready for application.

#### **4.6 Concept Applications**

The final results from the thesis workflow have the potential for application within many fields. Once integrated with additional geospatial data, such as building shapefiles, and incorporated into a GIS or other spatial analyses platform, the possible uses are only limited by the user (Figure 32). The degree of usefulness of the four geospatial datasets produced by this workflow depends on the field application. One or all of the output datasets from the workflow can be used in elements of each of the following fields: military operations, emergency response, humanitarian aid, topographic survey, and cultural heritage. The incorporation of the presented workflow in this thesis would assume the needs of the user require optimal 3D geospatial results while incurring minimal cost and training while having no internet access.

One of the most important requirements of geospatial data used for military operations is accuracy. Having precise and current information is paramount to all other factors of data [3], [31]. Secondary to data accuracy is the speed of data acquisition to analysis. Time-critical applications of geospatial information such as real-time tactical operations require cutting-edge technology far superior to anything available to the public [15]. Using the workflow presented in this project would produce products for much less time-sensitive scenarios. Having a broad imagery overview of an AOI or sparse point cloud provides geospatial information about a region that could otherwise be difficult to

infer from ground position. DEMs would provide relatively accurate elevation datasets, able to supplement movement operations and base camp set up.

Emergency response situations require rapid planning in situations where 3D data is not readily available. Some departments have incorporated aerial survey systems that provide real-time video feed of an AOI [8]. Attempts to advance this technology further into the realm of producing 3D datasets in an affordable manner have been researched [8]. Three primary factors needed for emergency response data acquisition are overall AOI spatial awareness, processing speed, and cost. Having knowledge of the scene is crucial for emergency responders. Without proper information the lives of those in danger as well as the responders are in jeopardy. The near-instant aerial imagery provided by this method would allow immediate visual review and improve situational response. Alternative aerial viewing angles of the AOI would broaden the scope of the emergency environment. Using the sparse 3D point cloud would elucidate structure or scene obstacles and allow them to be quickly modeled or analyzed. The textured 3D model might not be available for immediate use with emergency response, but could be incorporated into planning phases of emergency situations, such as wild fires [8]. Another significant factor for acquiring 3D geospatial data is the cost. Many emergency response units do not have overhead funding to acquire the equipment or datasets for 3D AOI models. For this reason, using an affordable workflow to acquire 3D geospatial data is ideal [8].

Humanitarian aid operations are large, complex orchestrations usually performed by non-profit organizations in regions of the world where modern technologies are not

readily available. In the instances of the earthquake in Haiti (2010) and Fukushima, Japan (2011), certain commercial satellite imagery companies offered continual and frequent imagery updates for the regions under duress under the International Charter on Space and Major Disasters ([www.disasterscharter.org](http://www.disasterscharter.org)). Even though satellite imagery is incredibly useful for high-level scene awareness, it does not provide detail about many ground structures or features. The lack of commercial-grade surveying equipment, or funding to acquire the equipment or 3D data, provide an ideal situation to apply this demonstrated workflow. Regions requiring humanitarian aid can experience a range of situations, such as natural disasters, drought or famine, and contagious diseases. Each of these scenarios requires geospatial information about the AOI. Aerial imagery would give aid workers an overview of the environmental situation or extent of damage in areas that are otherwise unable to be traversed on foot. Stitching the images together to create reference maps can aide with documenting evolving landscapes, such as refugee camps [50], [52]. Sparse 3D point clouds would model the scene in such a way that aid workers could quickly gain spatial awareness of objects within the AOI. The point cloud could also be used for quick 3D feature extraction, presenting a modeled recreation of the AOI. Using the sparse point cloud or a DEM from the geospatial data could significantly aid in determining locations for temporary aid camps or bivouacs. DEMs also offer data potentially used for identifying aerial med-evac or helipad operations. The textured 3D model could be used for wholesome environment representation. This model can be used for training, educating, and planning for aid workers as well as victims within the affected area. The affordability and accessibility of this workflow strongly adheres to the

confines within which humanitarian organizations are able to function. This workflow could be implemented in almost any situation worldwide with minimal funding and limited training.

Topographic surveys traditionally use planes or helicopters with LiDAR capabilities to produce large-scale geospatial datasets of regions. As cities and environments evolve, the subtle changes need to be documented. Ordering or performing frequent large-scale aerial LiDAR surveys is incredibly expensive and requires substantial equipment and training. Being able to perform a localized aerial survey with 3D data results comparable to LiDAR is very useful for topographic surveys [18], [17]. The research studies performed by Tonkin and Azmi reveal an ongoing interest in developing affordable and accessible methods of aerial surveying and production of 3D geospatial data. DEMs are foundational datasets used to create topographic surveys. Using the elevation data, maps and digital feature datasets are able to be accurately georectified and updated with current positioning. Topographic surveys rely on periodically updating their subject information. Using the 3D point clouds or texture model would supplement feature placement or alteration. The frequency of updating or modifying topographic surveys can be financially taxing [17]. The use of this workflow would greatly reduce the upkeep cost of continual aerial surveys.

Cultural heritage fields have a tendency to hold onto the past. Only recently have many research institutions involved with cultural heritage and archaeology adopted using digital means to document, record, and survey [58], [59]. Although the incorporation of modern technologies within cultural heritage has flourished in the past few years, many

groups are still pushing the limitations of cost and accessibility. The use of low-cost and accessible equipment for aerial surveying and acquisition of 3D geospatial data is a growing pursuit within cultural heritage [21], [22], [24]. Using aerial imagery has been a foundational aspect of archaeological excavations. The aerial perspective broadens the overall understanding of features and their relationships. The images can be stitched together to create an overview map which can be used for planning and education [50]. The sparse 3D point cloud is a rapid solution for giving relative spatial placement of features such as architectural ruins, burial sites, and historical landmarks. Additional features can be extrapolated from the sparse point cloud to create a 3D digital model for increased visibility. At the same time, the final texture model would provide a complete rendering of an object or AOI which can be used for planning, education, and publication. Cultural heritage foundations or research groups usually do not have guaranteed funding or overhead for expensive technologies. Using this workflow would offer an affordable solution to acquiring the much desired 3D geospatial data. Being accessible and customizable, the workflow can be altered to best suit individual parameters.

## CHAPTER FIVE: CONCLUSION & FUTURE RESEARCH

The process and applications of this thesis research present exciting opportunities for using low-cost and accessible aerial imagery platforms to create original 3D datasets. The relative ease of using simple aerial vehicles, cameras, and open source software suggest the thesis pipeline as a viable method for rapid 3D reconstruction. Reviewing the current literature and research journals reveals that the aerial imagery-SfM-3D reconstruction workflow is a highly desired method, and is pursued within the fields of computer vision, cultural heritage, topographic survey, emergency response, military intelligence, and more. Utilizing this thesis workflow can greatly contribute to research applications searching for accessible, affordable, and straight-forward methods for rapid 3D reconstruction from imagery, especially from aerial platforms.

The method of aerial imagery capture presented in this project is supplied as an affordable and easy-to-use solution that is widely accepted worldwide. Kites and balloons are traditionally viewed as innocuous or even friendly symbols [50]. Drones and UAVs are incredibly useful pieces of technology for aerial remote sensing, but often endure resistance due to their publicized use with military applications [60]. Only within the past few years have UAVs become viable as tools for private research and application [3]. Cutting-edge drone technology capable of remote sensing still remains prohibitive in terms of price and required piloting skill set. As remote-controlled and automated aerial

platforms continue to become more affordable and navigable, they will proliferate in use worldwide.

The resurgence of SfM as a means for 3D reconstruction available publicly for virtual tourism (Photosynth) and research (VisualSfM, Bundler) beckons to its simplicity and accessibility as a tool. Providing an affordable and accessible solution for 3D reconstruction is rapidly growing in public demand [2], [8], [21], [28]. Highly advanced systems of 3D reconstruction such as LiDAR involve sophisticated hardware, software, and vehicles to produce datasets. Even though LiDAR datasets are considered the optimal industry standard for 3D scene collection, they have severe limitations due to being expensive and technically challenging to capture and manage [18]. Until LiDAR becomes more accessible to general-use customers or easily captured without expensive equipment, SfM is widely used as a comparable solution.

There are a number of best practices to consider based on the results from this study, relating to aerial imagery quality, workflow stability, and 3D data integrity. For aerial image quality, it is necessary to use a vehicle that is reliable and will behave in a predictable manner when piloted. Most research performed through academia and citizen science regarding aerial kite imagery conclude that the delta shaped kite design provides the optimal lift and directional control for best results [50], [52]. The dual-line available with the sport kite used in this project provided additional control of the vehicle while reducing the stability of the platform. This result suggests that given equal weather conditions, a more stable kite could benefit the workflow by producing clear imagery due to less rapid movement. For the camera, there is no consensus on what device is optimal,

as the purpose for different cameras differs with the usage. The GoPro has been a common tool for many kite imaging enthusiasts as well as commercial UAV producers, due to it being high quality, lightweight, and equipped with numerous capturing features [50], [61], [62]. Most images captured are able to be processed by SfM algorithms as long as the image series adheres to the proper capture method (see section 3.2.3). Natural and man-made objects that appear in images such as buildings and vegetation can equally be identified within SIFT. There are features that present difficulties for aerial imagery capture, SfM algorithms, and 3D modeling, which should be avoided. Moving, reflective, thin, or amorphous features, such as water, clouds, mirrors, power lines, or bare tree branches are considered anomalies and will usually cause substantial errors within SfM, which subsequently misleads 3D reconstruction. The primary open source software used in this project (VisualSfM, MeshLab) were chosen due to their broad support and appearance in related scientific journals. Other similar open source software platforms that are used are Bundler and Blender, for SfM and 3D modeling, respectively. Throughout all the literature reviewed no single software platform mentioned above was clearly revealed as superior. In fact, most articles that chose to use one platform, such as Bundler, often mentioned the corresponding platform (VisualSfM) as a viable and respected option. The best practice solutions for an open source software SfM to 3D model pipeline are the four platforms mentioned: VisualSfM, Bundler, MeshLab, and Blender. For ideal 3D data results and accuracy integrity it is best to have proper ground control and scene measurements. Unless relative measurements or exact coordinates are known, any survey performed risks the 3D data being misleading. Best practice for

survey accuracy is to perform research or capture precise ground control coordinates. Additional research must be performed to test the workflow in various field survey conditions. According to the conclusions from this project, open fields with limited visual obstructions provide optimal results. Kite aerial imagery communities suggest that most locations are able to be surveyed as long as terrain provides enough room for takeoff and landing, vertical obstructions are limited, and weather conditions are favorable [50].

### **Future Research**

The workflow executed in this thesis proved a working demonstration of rapidly creating 3D geospatial data from aerial imagery using open source SfM. Future research regarding this thesis project will focus around potential improvements and alternative equipment or methods. In this section alternative options for equipment and software improvement and survey location testing are discussed, as well as future implications for aerial surveying.

An ideal camera platform for this project would be a high-resolution device with increased capacity to stream live pictures or video feed to a workstation. This camera would improve the speed and quality of images used in the following SfM process and texture model. In addition, a GPS device with increased elevation reading would contribute additional data towards later analysis for positional placement of the data. It would also be beneficial to incorporate a small laser range finder onto the aerial platform to have distance readings between the platform and observed scene. In addition, using a stabilizing device such as a gimbal on the camera would greatly improve stability.

Stabilized images would be clearer and more unified which produces higher fidelity SfM results and improved optical accuracy.

GPS devices and precise ground control points would greatly increase the accuracy of this workflow. Measuring relatively the results of this project produce exceptional data, but with increased geospatial accuracy the 3D data becomes more useful. Including a brief step in the workflow for capturing ground coordinates through GPS or surveying would provide the necessary information for scene calibration. In addition, using a range finder or laser measurements could provide quick benchmarks for observer placement.

A simple alteration to the project workflow is to increase the altitude of the kite. A higher altitude would reveal a farther view distance and allow the AOI to be captured in fewer images. For the project the kite remained at an altitude ranging between 60 and 100 feet depending on wind speed. The average height estimated during the project was around 70 feet, with the useful observable distance calculated at less than 100 feet away from the sensor at ground level with a field of view limited to the size of the camera lens (see section 4.2). The FAA regulations state the maximum altitude for an anchored aerial vehicle cannot exceed 500 feet. Equipping the kite with 500 feet of string would allow a very large field of view to be captured (Figure 33). Estimating the maximum oblique angle for the camera at around  $45^\circ$ , a kite altitude of 500 feet could produce images with a useable view distance of around 600 to 700 feet. The altitude would detract from the camera's ability to capture detailed images. Being far from the photographed objects would also require a very large change in angle of the kite in order to achieve a useable

perspective difference between the image series. Depending on the desired use for the images or workflow results, having such a large AOI angle could potentially produce illuminating area surveys.



**Figure 33 - 500 ft kite altitude**

Using innocuous and simple aerial vehicles such as kites and balloons is a suitable means to acquire aerial imagery. Piloting a kite for this project was useful for proving the workflow demonstration, but more advanced aerial vehicles and methods are available. The more advanced an aerial platform becomes, usually expense and operation difficulty increase. This is true for UAVs within the \$100 to \$600 range because they require manual piloting and have reduced capabilities. Once the price goes above \$600, commercial UAVs become highly-tuned with extensive capabilities. The most significant technological advancement for these commercial UAVs is the autopilot ability.

There are a handful of UAVs that may be considered for integration with this research workflow. The combination of reasonable pricing and impressive aerial capabilities are promising for these platforms, the 3D IRIS and DJI Phantom. The 3D IRIS produced by 3D Robotics (3DR) is a quadcopter with the lift capacity to carry 0.8 lbs, two-axis gimbal stabilization, built-in carrier for a digital camera, and maintain over 20 minutes of flight time [62]. These specifications alone meet minimum desired requirements for carrying additional camera gear and performing numerous surveys. The most significant capability of the 3D IRIS is its 3DR-developed autopilot function which allows the UAV to automatically navigate to its given destination. The 3D IRIS is made in America and is available for \$750. The DJI Phantom produced by DJI is a quadcopter with a built-in high-resolution camera, automatic takeoff and landing functions, live video feeds from the UAV, and onboard sensors for obstacle detection [61]. Although the Phantom does not have autopilot capability for traversing, it still maintains the ability to correct itself and refrain from crashing into obstructions. The live video feed and built-in camera are maximally integrated to produce precise survey results. The Phantom is available for around \$900. These aerial systems single-handedly address the limitations faced by most UAV imaging methods: being able to adequately survey an area due to aerial vehicle mobility, and vehicle navigation precision which is usually severely limited by the pilot. Less than seven years ago, UAVs with a fraction of these capabilities and precision were very uncommon with pricing around \$7,000, which was still considered “affordable” by some purchasers [8].

It is very possible to use proprietary SfM solutions such as Photosynth and 123D Catch within the workflow presented in this thesis. The primary reasons for not using them in this research are their limitation on parameter customization, photograph restrictions, black-box algorithms, and internet reliance. Within a controlled research environment it is entirely possible and encouraged to use all available tools at your disposal. The limitations of applying the workflow in the field discouraged the use of these packages as possible solutions. For future applications, incorporating Photosynth and 123D Catch as potential SfM solutions could improve output integrity and processing speed.

Other locations of interest should be considered for aerial survey. Optimally, survey locations focusing on distinct features would allow the thesis methods to be fully tested. Surveys sites such as an empty field, clustered buildings, dense vegetation, or rough terrain would all present unique circumstances for the workflow to attempt. For some of these environments the use of navigable aerial platforms or UAVs would likely have to be used.

When it comes to SfM the most limiting factor is processing time. Using the standard incremental reconstruction SfM method has the limitations of loops and initializations, which create a geometric increase in processing time. Incremental reconstruction is necessary when image series are seemingly random or do not have predefined relationships established. Using the workstation in this project, performing SfM took about 3 minutes for 40 photos, and 20 minutes for 160 images. This progression of processing time portrays the geometric processing time required by using

incremental reconstruction. Optimal solutions would be to use powerful processors or even cloud computing services to calculate the SfM results. Powerful processors are more expensive and cloud computing requires at least a temporary internet connection.

Monetary expense and internet reliability are both intentionally avoided in this project to prove an affordable and accessible workflow concept. One solution that can be integrated into the current workflow is the use of linear SfM processing [39]. Linear SfM processing implies that the image series was captured in sequential order, therefore assuming that each image is adjacent to the next. The linear SfM algorithm significantly reduces processing time due to each image only being compared to the implied nearest neighbors, effectively increasing time for each added image by a constant, linear amount.

An interesting element to research and apply to this workflow is a crowd-sourced approach [63]. The advantage of SfM is its ability to aggregate images from multiple camera sources with different parameters or even images captured at varying times and conditions. This strength of SfM would play well into attempting a crowd-sourced approach to the workflow. Multiple aerial vehicles and ground units could simultaneously capture images of the AOI and place them in a single repository. VisualSfM would be capable of managing the image series and potentially utilizing a majority of the images to produce the point cloud result. A crowd-sourced approach could greatly increase the speed of survey imagery capture and variety of AOI perspectives, resulting in a higher fidelity point cloud and 3D model. Crowd sourcing would also allow image contributions to be added to the image series at different times. With each subsequent or additional crowd-sourced survey, the image series would grow in complexity and detail. In a similar

manner using multiple cameras either on the aerial vehicle or with multiple vehicles would significantly improve overall coverage and potential images for the AOI. Further research would be performed to determine the proper distributed system upon which the crowd-sourced method would depend.

Another interesting element related to the use of SfM comes from the approach that 123D Catch advertises. AutoCAD's SfM software is advertised as a solution for digitally capturing objects and using their software pipeline to produce 3D models from a 3D printer. 3D printers have only recently become available for public use within the past few years, previously only available with industrial applications. These devices offer novel and practical solutions for creating plastic recreations of objects. Using the 3D model results from this workflow, miniature models of the surveyed AOI could be produced using 3D printers. Having a tangible recreation of a surveyed area enhances the perception and information communicated. With a complete workflow in place along with a 3D printer, it would be possible to survey, process, and produce a 3D physical model of an AOI within hours of initiation.

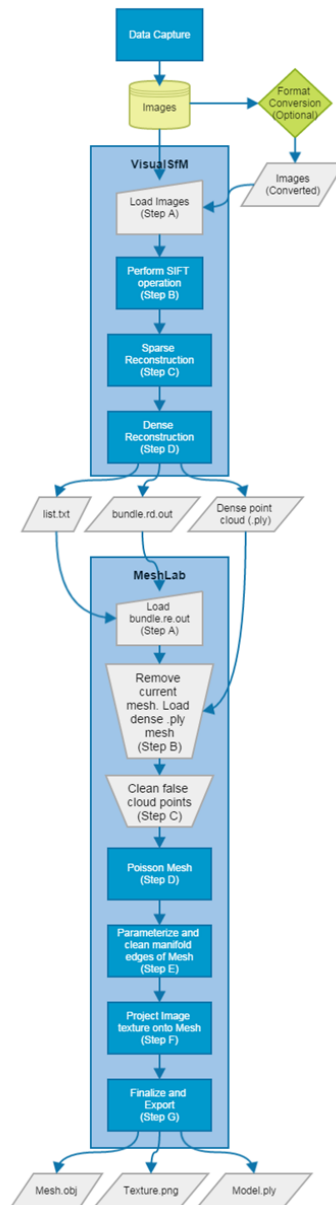
Perhaps the most significant issue surrounding this research and related fields is increased public awareness of aerial vehicles such as UAVs and their impacts on safety and privacy. The introduction of UAVs as serious surveillance and weapon delivery systems emerged during the first Gulf War, according to a Department of the Navy report in 1991. Military or government agency functions for UAVs were proprietary until recent adaptations of UAVs became available for public use. The legality of recreational and professional UAVs is currently under debate by the FAA [66]. The ruling from the FAA

could either expand or cripple the use of UAVs in the public domain. The current FAA regulations concerning UAVs do not address the issues of privacy or surveillance, as long as the vehicle is used for the intended recreational purpose. Drones may not be used for commercial purposes. Consequently, a common public perception of UAVs is drawn from the military aspect instead of the research and utility potential UAVs have. This perception along with the increased public awareness of developing privacy concerns has caused an uncharted realm for legal and public debate over UAVs. The growth of the internet in the past few decades produced debates and concepts of privacy and individual rights that were never previously imagined in legal terms. Especially with the proliferation of social media and mobile sensors, an individual's location and information privacy are almost nonexistent. Surprisingly, most people do not even realize they are usually broadcasting such private information [64]. This fact causes companies and legislatures to consider whether or not the legality of location-based information is considered private depending if you are in a private or public location. Projects such as Google Street View are ground-breaking in their ingenuity and ability to capture geospatial data. Very soon after its inception and public reveal, Google was under fire for potentially violating the privacy of every location and person the project mapped. Although Google legally acquired all Street View imagery and is allowed to publically display it online, many people still believe their privacy is violated. During some of the Street View project, Google "casually" acquired wifi signals, emails, and passwords of nearby homes, resulting in a legal suit presented by 38 US states and a fine of 7 million dollars [65]. With Google and many technologies pushing the limits of public and private

data, it is not surprising when the concept of highly-mobile aerial vehicles (with a marred history of military affiliation) equipped with cameras or other sensors being abundant are questioned. With the future of UAVs being uncertain, using more acceptable aerial vehicles such as kites and balloons would rarely cause vitriol or concern for privacy or safety.

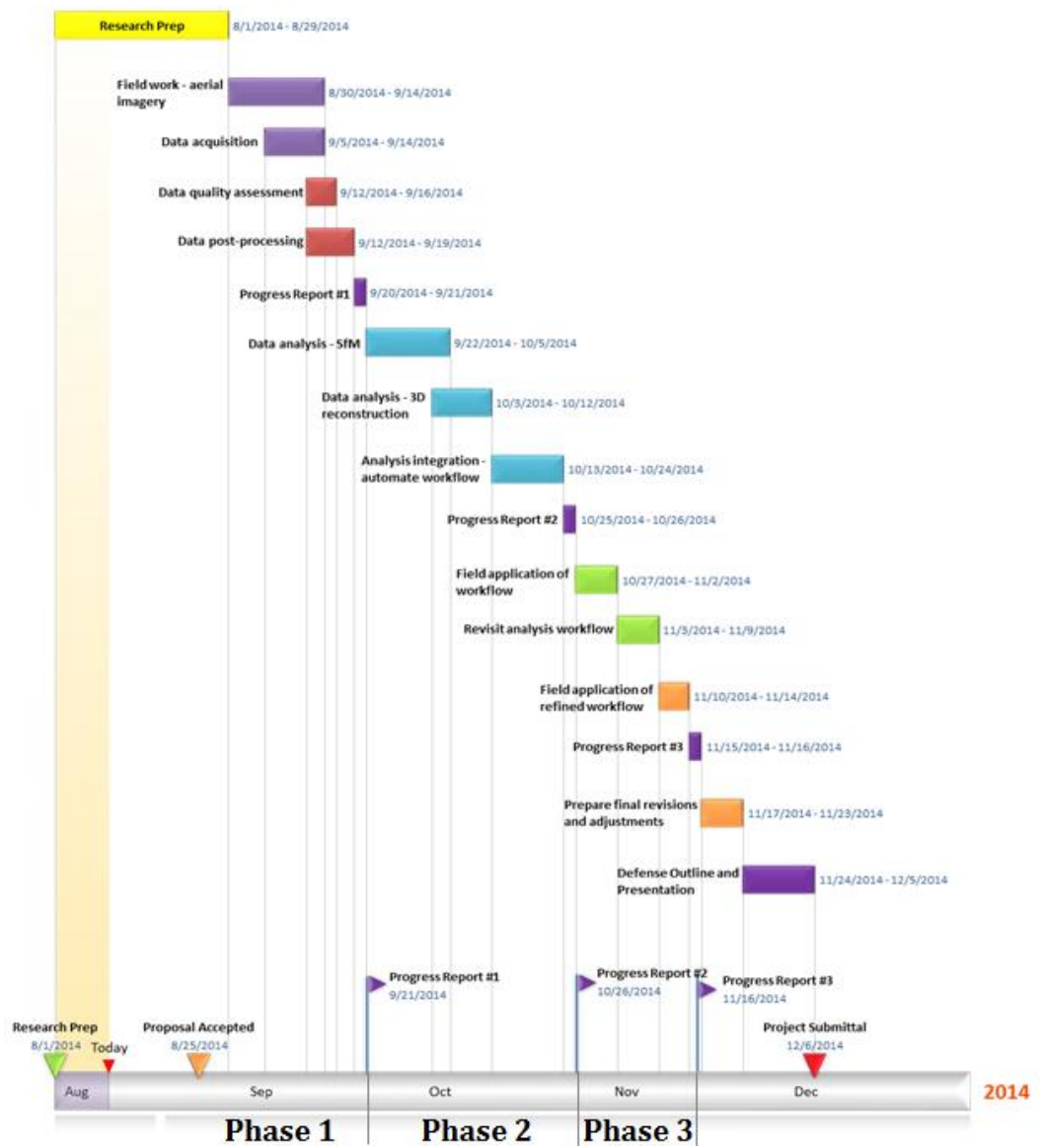
## APPENDIX A

Complex workflow



## APPENDIX B

### Project Schedule



## REFERENCES

- [1] H. Zhang, B. Li, J. Zhang, and F. Xu, "Aerial Image Series Quality Assessment," *IOP Conf. Ser. Earth Environ. Sci.*, vol. 17, p. 012183, Mar. 2014.
- [2] B. Ducke, D. Score, and J. Reeves, "Multiview 3D reconstruction of the archaeological site at Weymouth from image series," *Comput. Graph.*, vol. 35, no. 2, pp. 375–382, Apr. 2011.
- [3] I. Colomina and P. Molina, "Unmanned aerial systems for photogrammetry and remote sensing: A review," *ISPRS J. Photogramm. Remote Sens.*, vol. 92, pp. 79–97, Jun. 2014.
- [4] R. Samar and W. A. Kamal, "Optimal Path Computation for Autonomous Aerial Vehicles," *Cogn. Comput.*, vol. 4, no. 4, pp. 515–525, Dec. 2012.
- [5] A. S. Saif, A. S. Prabuwo, and Z. R. Mahayuddin, "Real time vision based object detection from UAV aerial images: a conceptual framework," in *Intelligent Robotics Systems: Inspiring the NEXT*, Springer, 2013, pp. 265–274.
- [6] L. Evers, T. Dollevoet, A. I. Barros, and H. Monsuur, "Robust UAV mission planning," *Ann. Oper. Res.*, vol. 222, no. 1, pp. 293–315, Nov. 2014.
- [7] S. Kahn, "Reducing the gap between Augmented Reality and 3D modeling with real-time depth imaging," *Virtual Real.*, vol. 17, no. 2, pp. 111–123, Jun. 2013.
- [8] G. Lewis, "Evaluating the use of a low-cost unmanned aerial vehicle platform in acquiring digital imagery for emergency response," in *Geomatics solutions for disaster management*, Springer, 2007, pp. 117–133.
- [9] W. Yi and L. Özdamar, "A dynamic logistics coordination model for evacuation and support in disaster response activities," *Eur. J. Oper. Res.*, vol. 179, no. 3, pp. 1177–1193, Jun. 2007.
- [10] R. Margesson and M. Taft-Morales, "Haiti Earthquake: Crisis and Response," Feb. 2010.

- [11] M. Buchroithner, N. Prechtel, and D. Burghardt, Eds., *Cartography from Pole to Pole*. Berlin, Heidelberg: Springer Berlin Heidelberg, 2014.
- [12] K. P. Valavanis and G. J. Vachtsevanos, Eds., *Handbook of Unmanned Aerial Vehicles*. Dordrecht: Springer Netherlands, 2015.
- [13] U. Isikdag, Ed., *Innovations in 3D Geo-Information Sciences*. Cham: Springer International Publishing, 2014.
- [14] L.-C. Chen, T.-A. Teo, C.-H. Hsieh, and J.-Y. Rau, "Reconstruction of building models with curvilinear boundaries from laser scanner and aerial imagery," in *Advances in Image and Video Technology*, Springer, 2006, pp. 24–33.
- [15] M. Kampouraki, G. A. Wood, and T. R. Brewer, "Opportunities and limitations of object based image analysis for detecting urban impervious and vegetated surfaces using true-colour aerial photography," in *Object-Based Image Analysis*, Springer, 2008, pp. 555–569.
- [16] K. C. Clarke, "Why simulate cities?," *GeoJournal*, vol. 79, no. 2, pp. 129–136, Apr. 2014.
- [17] T. N. Tonkin, N. G. Midgley, D. J. Graham, and J. C. Labadz, "The potential of small unmanned aircraft systems and structure-from-motion for topographic surveys: A test of emerging integrated approaches at Cwm Idwal, North Wales," *Geomorphology*, vol. 226, pp. 35–43, Dec. 2014.
- [18] S. M. Azmi, B. Ahmad, and A. Ahmad, "Accuracy assessment of topographic mapping using UAV image integrated with satellite images," *IOP Conf. Ser. Earth Environ. Sci.*, vol. 18, p. 012015, Feb. 2014.
- [19] D. Crandall, A. Owens, N. Snavely, and D. Huttenlocher, "Discrete-continuous optimization for large-scale structure from motion," in *Computer Vision and Pattern Recognition (CVPR), 2011 IEEE Conference on*, 2011, pp. 3001–3008.
- [20] J. Bourgeois and M. Meganck, *Aerial Photography and Archaeology 2003: A Century of Information ; Papers Presented During the Conference Held at the Ghent University, December 10th - 12th, 2003*. Academia Press, 2005.
- [21] M. Block, "Project Archaeocopter." 2014. [Online]. Available: <http://www.archaeocopter.de/>
- [22] C. Corsi, B. Slapšak, and F. Vermeulen, *Good Practice in Archaeological Diagnostics: Non-invasive Survey of Complex Archaeological Sites*. Springer Science & Business Media, 2013.

- [23] C. Corsi, B. Slapšak, and F. Vermeulen, Eds., *Good Practice in Archaeological Diagnostics*. Cham: Springer International Publishing, 2013.
- [24] “3D archaeology - now low-cost, high-volume and crowd-sourced.” .
- [25] N. Snavely, S. M. Seitz, and R. Szeliski, “Photo Tourism: Exploring Photo Collections in 3D,” in *ACM SIGGRAPH 2006 Papers*, New York, NY, USA, 2006, pp. 835–846.
- [26] ISTI-CNR, “MeshLab,” *MeshLab*, 2014. [Online]. Available: <http://meshlab.sourceforge.net/>.
- [27] J. L. Carrivick, M. W. Smith, D. J. Quincey, and S. J. Carver, “Developments in budget remote sensing for the geosciences,” *Geol. Today*, vol. 29, no. 4, pp. 138–143, Jul. 2013.
- [28] M. A. Fonstad, J. T. Dietrich, B. C. Courville, J. L. Jensen, and P. E. Carbonneau, “Topographic structure from motion: a new development in photogrammetric measurement,” *Earth Surf. Process. Landf.*, vol. 38, no. 4, pp. 421–430, Mar. 2013.
- [29] “CHNT 18, 2013 – Abstracts | CHNT | Vienna.” .
- [30] M. J. Smith, J. Chandler, and J. Rose, “High spatial resolution data acquisition for the geosciences: kite aerial photography,” *Earth Surf. Process. Landf.*, vol. 34, no. 1, pp. 155–161, Jan. 2009.
- [31] S. \_Harwin and A. Lucieer, “Assessing the Accuracy of Georeferenced Point Clouds Produced via Multi-View Stereopsis from Unmanned Aerial Vehicle (UAV) Imagery,” *Remote Sens.*, vol. 4, no. 6, pp. 1573–1599, May 2012.
- [32] James S. Aber, I. Marzoff, and J.B. Ries, *Small-format Aerial Photography: Principles, Techniques and Geoscience Applications*. Amsterdam: Elsevier, 2010.
- [33] E. Mouragnon, M. Lhuillier, M. Dhome, F. Dekeyser, and P. Sayd, “Generic and real-time structure from motion using local bundle adjustment,” *Image Vis. Comput.*, vol. 27, no. 8, pp. 1178–1193, Jul. 2009.
- [34] Microsoft, *Photosynth*, 2014. [Online]. Available: <https://photosynth.net/>.
- [35] AutoCAD, *123D Catch*, 2014. [Online]. Available: <http://www.123dapp.com/catch>.

- [36] Yasutaka Furukawa, “Clustering Views for Multi-view Stereo,” *IEEE Trans. Pattern Anal. Mach. Intell.*, vol. Vol. 32, no. Issue 8, p. Pages 1362–1376, Aug. 2010.
- [37] Yasutaka Furukawa, *Patch-based Multi-view Stereo Software*, 2014. [Online]. Available: <http://www.di.ens.fr/pmvs/>.
- [38] Changchang Wu, “VisualSFM: A Visual Structure from Motion System,” *VisualSFM: A Visual Structure from Motion System*, 2011. [Online]. Available: <http://ccwu.me/vsfm/>.
- [39] Changchang Wu, “Towards Linear-time Incremental Structure From Motion,” *3DV*, 2013.
- [40] Changchang Wu, Sameer Agarwal, Brian Curless, and Steven M. Seitz, “Multicore Bundle Adjustment,” *CVPR*, 2011.
- [41] D. G. Lowe, “Distinctive Image Features from Scale-Invariant Keypoints,” *Int. J. Comput. Vis.*, vol. 60, no. 2, pp. 91–110, Nov. 2004.
- [42] G. Pomaska, “Utilization of photosynth point clouds for 3D object reconstruction,” in *Proceedings of the 22nd CIPA symposium, Kyoto, Japan*, 2009.
- [43] Y. Yu, K. Zhou, D. Xu, X. Shi, H. Bao, B. Guo, and H.-Y. Shum, “Mesh editing with poisson-based gradient field manipulation,” in *ACM Transactions on Graphics (TOG)*, 2004, vol. 23, pp. 644–651.
- [44] J. Tohline, “Origin of the poisson equation.” 1999.
- [45] M. Kazhdan, M. Bolitho, and H. Hoppe, “Poisson surface reconstruction,” in *Proceedings of the fourth Eurographics symposium on Geometry processing*, 2006.
- [46] W. E. Lorensen and H. E. Cline, “Marching Cubes: A High Resolution 3D Surface Construction Algorithm,” in *Proceedings of the 14th Annual Conference on Computer Graphics and Interactive Techniques*, New York, NY, USA, 1987, pp. 163–169.
- [47] F. Bernardini, J. Mittleman, H. Rushmeier, C. Silva, and G. Taubin, “The ball-pivoting algorithm for surface reconstruction,” *IEEE Trans. Vis. Comput. Graph.*, vol. 5, no. 4, pp. 349–359, Oct. 1999.
- [48] N. Amenta, S. Choi, and R. K. Kolluri, “The power crust, unions of balls, and the medial axis transform,” *Comput. Geom.*, vol. 19, no. 2–3, pp. 127–153, Jul. 2001.

- [49] T. K. Dey and S. Goswami, “Tight Cocone: A Water-tight Surface Reconstructor,” in *Proceedings of the Eighth ACM Symposium on Solid Modeling and Applications*, New York, NY, USA, 2003, pp. 127–134.
- [50] “Public Lab,” *Kite Mapping*, 2014. [Online]. Available: <http://publiclab.org/wiki/kite-mapping>.
- [51] *e-CFR: Title 14: Aeronautics and Space*, vol. Part 101. .
- [52] Mendeley Group, “Kite Aerial Photography.” 2014. [Online]. Available: <http://www.mendeley.com/groups/1225421/kite-aerial-photography-kap/papers/>
- [53] Jesse, “We Did Stuff,” *Open Source Photogrammetry: Ditching 123D Catch*, 12-Jul-2013. [Online]. Available: <http://wedidstuff.heavyimage.com/index.php/author/admin/>.
- [54] Changchang Wu, “VisualSfM : A Visual Structure from Motion System,” *VisualSfM : A Visual Structure from Motion System*, 2014. [Online]. Available: <http://ccwu.me/vsfm/doc.html>.
- [55] VisualSize, “How to Take Pictures for Photomodel3D,” *How to Take Pictures for Photomodel3D*, 2014. [Online]. Available: <http://www.visualsize.com/FAQ/3Dmodel.php>.
- [56] iromu, “VisualSfM OSX app builder,” *GitHub*, 2014. [Online]. Available: <https://github.com/iromu/vsfm-osx>.
- [57] Scott Sawyer, “Building VisualSfM on Ubuntu 12.04 (Precise Pangolin) Desktop 64-bit,” *10Flow*, 15-Aug-2012. [Online]. Available: <http://www.10flow.com/2012/08/15/building-VisualSfM-on-ubuntu-12-04-precise-pangolin-desktop-64-bit/>.
- [58] David Schloen, Sandra Shloen, Miller Prosser, and Charles Blair, “OCHRE Data Service,” *OCHRE Data Services*, 2014. [Online]. Available: <https://ochre.sites.uchicago.edu>.
- [59] Leon Levy, “Leon Levy Foundation,” *Leon Levy Foundation*, 2014. [Online]. Available: <http://leonlevyfoundation.org/>.
- [60] N. Sharkey, “The Automation and Proliferation of Military Drones and the Protection of Civilians,” *Law Innov. Technol.*, vol. 3, no. 2, pp. 229–240, Dec. 2011.
- [61] DJI, “Phantom,” *DJI*, 2014. [Online]. Available: <http://www.dji.com/product/phantom>.

- [62] 3DRobotics, "IRIS+," *3DRobotics*, 2014. [Online]. Available: <http://store.3drobotics.com/products/IRIS>.
- [63] Andrew Bevan, "3D archaeology - now low-cost, high-volume and crowd-sourced," *3D Archaeology*, 23-Jul-2014. [Online]. Available: <http://www.software.ac.uk/blog/2014-07-23-3d-archaeology-now-low-cost-high-volume-and-crowd-sourced>.
- [64] G. Friedland and R. Sommer, "Cybercasing the Joint: On the Privacy Implications of Geo-Tagging.," in *HotSec*, 2010.
- [65] D. Streitfeld, "Google Admits Street View Project Violated Privacy," *The New York Times*, 12-Mar-2013.
- [66] "Unmanned Aircraft Systems." [Online]. Available: <https://www.faa.gov/uas/>. [Accessed: 05-Dec-2014].

## **BIOGRAPHY**

Michael Roy Resig graduated from Horseheads High School, Horseheads, New York, in 2005. He received his Bachelor of Arts from Wheaton College, IL in 2009. He was an active volunteer and employed as a GIS Specialist by the Leon Levy Archaeological Expedition to Ashkelon, Israel for three seasons. He is a geospatial engineer and analyst for Northrop Grumman. He earned his Master of Science in Geoinformatics and Geospatial Intelligence from George Mason University in 2014.